SPRINGER BRIEFS IN MOLECULAR SCIENCE

Masahiro Kinoshita

Mechanism of Functional Expression of the Molecular Machines

Springer

SpringerBriefs in Molecular Science

More information about this series at http://www.springer.com/series/8898

Masahiro Kinoshita

Mechanism of Functional Expression of the Molecular Machines

Springer

Masahiro Kinoshita
Institute of Advanced Energy
Kyoto University
Kyoto
Japan

ISSN 2191-5407 ISSN 2191-5415 (electronic)
SpringerBriefs in Molecular Science
ISBN 978-981-10-1484-0 ISBN 978-981-10-1486-4 (eBook)
DOI 10.1007/978-981-10-1486-4

Library of Congress Control Number: 2016942489

Printed on acid-free paper

This Springer imprint is published by Springer Nature
The registered company is Springer Science+Business Media Singapore Pte Ltd.

Preface

In this book, we briefly discuss the mechanism of functional expression of a protein or protein complex utilizing the ATP hydrolysis cycle or proton-motive force from a unique point of view which has not yet been adopted. We consider a variety of processes such as the unidirectional movement of a linear-motor protein along a filament, insertion of an unfolded protein into a chaperonin and release of the folded protein from it, transport of diverse substrates across the membrane by a transporter, and directed rotation of the central subunit within a rotatory-motor protein complex. It is shown that water plays imperative roles in the functional expression of these molecular machines. A pivotal factor is the entropic effect, force, or potential originating from the translational displacement of water molecules coexisting with the molecular machines in the entire system. It is pointed out that the processes mentioned above (they are referred to as "ordering processes" in this book) and the self-assembly processes such as protein folding and association can be comprehended in a unified manner within the same theoretical framework. The differences between the ordering and self-assembly processes are also discussed. The basic concept can be understood without consulting the references given, but for more details the readers should refer to them.

Masahiro Kinoshita

Acknowledgments

The author thanks all of the collaborators listed in the References. Sincere appreciation should be expressed to Dr. Satoshi Yasuda (Chiba University) for his critical reading of the draft and to Profs. Akihisa Shioi (Doshisha University) and Akira Yoshimori (Niigata University) for valuable comments on the ATP-driven proteins. The studies described in this book were supported by a Grant-in-Aid for Scientific Research on Innovative Areas (No. 20118004) from the Ministry of Education, Culture, Sports, Science and Technology of Japan and by a JSPS (Japan Society for the Promotion of Science) Grant-in-Aid for Scientific Research (B) (No. 25291035).

Contents

Chapter 1
Introduction

Abstract A variety of self-assembly and ordering processes are sustaining life. They are microscopic, mesoscopic, or macroscopic. In this book, we are concerned with the microscopic processes. We raise the following two questions: (1) It appears that the processes occur at a great expense of entropy, but is this true?; and (2) how is water imperative in life phenomena? Upon the processes, the entropy is considerably lowered if one looks at only the biomolecules. When the effect of water is taken into account to its full extent, matters become substantially different.

Keywords Life · Self-assembly · Ordering · Entropy · Biomolecule · Water

Understanding *life phenomena* is one of the most challenging issues in modern science. We have to solve multilevel problems in studies on life phenomena. The subjects to be tackled are properties and functions of a biomolecule, an ensemble of biomolecules, a cell, an organ or system comprising a number of cells, and a living body. A variety of processes which are microscopic, mesoscopic, and macroscopic are sustaining life. In this book, we are concerned solely with those of a microscopic scale which occur by a single biomolecule or several biomolecules. Their typical examples are protein folding, molecular recognition, association of proteins forming an ordered and often symmetrical complex, unidirectional movement of a linear-motor protein along a filament, insertion of an unfolded protein into a chaperonin and release of the folded protein from it, transport of diverse substrates across the membrane by an ATP-binding cassette (ABC) transporter, directed rotation of the central subunit within a rotatory-motor protein complex, and functional rotation of AcrB in a drug efflux pump. The key words representing these processes could be “self-assembly,” “ordering,” “high selectivity,” “regularity,” and “symmetry” which clearly contradict the principle of entropy increase for an isolated system in thermodynamics.

Some researchers believe that any biological process can be understood only as a nonequilibrium one in an open system. However, this is not necessarily correct

M. Kinoshita, *Mechanism of Functional Expression of the Molecular Machines*,
SpringerBriefs in Molecular Science, DOI 10.1007/978-981-10-1486-4_1

because many biological self-assembly and ordering processes at microscopic levels occur in closed, equilibration experiments performed at a laboratory. The concept of "dissipative structure" developed by Kondepudi and Prigogine [1] is not relevant to them. (The problems of the cell level and larger scales are expected to require the concept of dissipative structure.) They can be argued on the basis of equilibrium thermodynamics for a closed system. The most important quantity is the free energy becoming lower for any process occurrence. The free energy change ΔG is given as "$\Delta H - T\Delta S$" where ΔH and ΔS are the enthalpy and entropy changes, respectively, and T is the absolute temperature. It is generally believed that the processes mentioned above occur at a great expense of entropy but with a great lowering of enthalpy and that the latter dominates: $\Delta S \ll 0$, $\Delta H \ll 0$, and $|\Delta H| > |T\Delta S|$. Here is question number 1: Do they truly occur at a great expense of entropy?

When each of biomolecules, a great diversity of molecular and ionic species, and water is separately present, it is simply *material*. When they form a system, however, the complex correlations among these material constituents can lead to *life*. Above all, water should play critical roles. A larva of the sleeping chironomid living in Africa synthesizes trehalose when water is lost [2]. Through the glassification of trehalose the larva freezes its biological system and stops the metabolism, waiting for water supply. It is now material. Even after many years, when the insect is immersed in water, it returns to life and begins to live again. This is a striking example showing that life can be converted to material and vice versa and that water is indispensable to life. Here is question number 2: How is water imperative in life phenomena?

The purpose of this book is to give interesting answers to the two questions raised above. Such processes as protein folding, receptor-ligand or protein–protein binding, and protein association are categorized as "self-assembly processes," whereas the processes like the unidirectional movement of a linear-motor protein, insertion and release of a solute into and from a protein complex, and directed or functional rotation found in a protein complex are categorized as "ordering processes." Based on the results of our detailed analyses using statistical-mechanical theories, we argue that a self-assembly process is driven primarily by an entropic effect originating from the translational displacement of coexisting water molecules (not only the water molecules near the biomolecular surfaces but also those in the bulk). Upon a self-assembly process, a large gain of the translational, configurational entropy of water occurs and this gain predominates over the conformational-entropy loss of biomolecules. The proteins or protein complexes functioning in the ordering processes are often referred to as "molecular machines." It is shown that the entropic effect, force, or potential originating from the translational displacement of water molecules coexisting with the molecular machines play essential roles. The significance of ATP hydrolysis and proton motive force utilized by the molecular machines is also discussed from a unique viewpoint.

References

1. D. Kondepudi, I. Prigogine, *Modern Thermodynamics: From Heat Engines to Dissipative Structures*, 2nd edn. (Wiley, 2015)
2. M. Sakurai, T. Furuki, K. Akao, D. Tanaka, Y. Nakahara, T. Kikawada, M. Watanabe, T. Okuda, Proc. Natl. Acad. Sci. U.S.A. **105**, 5093 (2008)

Chapter 2
Importance of Translational, Configurational Entropy of Water

Abstract We argue that a self-assembly process occurs primarily to increase the system entropy. The water entropy increases whereas the conformational entropy of biomolecules decreases, and the increase is larger than the decrease. In many cases, the ordering processes can successfully be described by the potential of mean force induced between biomolecules or a solute and a biomolecule, in particular, its entropic component. The entropic effect or potential originates from the translational displacement of water molecules coexisting with biomolecules in the entire system: The conventional view looking at only the water near the biomolecular surface is inadequate. The hydration entropy of a biomolecule, the loss of water entropy upon biomolecule insertion, plays crucially important roles. The calculation of this quantity with sufficient accuracy is a central issue.

Keywords Self-assembly · Hydration entropy · Ordering · Potential of mean force · Hydration entropy

2.1 Biological Self-assembly Processes

Typical examples of microscopic, biological self-assembly processes are protein folding, protein traffic, ordered aggregation of proteins, and molecular recognition [1]. In protein folding, a long polypeptide chain folds into a unique structure called "native structure." There are many different species of proteins, and surprisingly enough, each of them knows where and how to go [1]. This is called "protein traffic." When proteins aggregate, ordered and often symmetrical structure is formed. A protein such as an enzyme binds only to a particular ligand. That is, the enzyme discriminates the ligand from the others, and it has very high ability of molecular recognition. There is another type of molecular recognition where an intrinsically disordered protein (IDP), which does not fold when it is isolated, forms a well-defined structure only when it binds to a target protein [2, 3]. An IDP often recognizes multiple targets, and its well-defined structure

M. Kinoshita, *Mechanism of Functional Expression of the Molecular Machines*,
SpringerBriefs in Molecular Science, DOI 10.1007/978-981-10-1486-4_2

formed is target dependent. The membrane is completed by the penetration of proteins into the lipid bilayer. It is surprising that each protein species knows where to penetrate [1].

2.2 Biological Ordering Processes

There is a class of proteins called "ATP-driven proteins" sharing the feature that they utilize the ATP hydrolysis cycle, that is, ATP binding to the protein, hydrolysis of ATP within it, and dissociation of the products, Pi and ADP, from it. A linear-motor protein [4] moves only in one direction along a filament similar in function to a railway track. Its movement is not random but unidirectional. The γ-subunit within F_1-ATPase exhibits directed rotation [5, 6]. An ABC transporter [7] excludes a toxic solute (substrate or drug) from a cell. It first inserts the drug and then releases it. An unfolded protein is inserted into a chaperonin [8] from bulk aqueous solution, and after the folding is finished within the chaperonin, the folded protein is released back to the bulk solution. It is quite mysterious that the two apparently opposite events, insertion and release, successively occur in the same system. There is another class of proteins utilizing the proton motive force (i.e., transfer of a proton from the higher-concentration side to the lower-concentration one). A good example is the drug efflux pump, AcrA/AcrB/TolC [9, 10]. The processes like the unidirectional movement, insertion/release events, and directed or functional rotation are categorized as "ordering processes" in this book. We argue that these processes and the self-assembly processes mentioned in Sect. 2.1 can be treated in a unified manner within the same theoretical framework.

An ABC transporter and AcrA/AcrB/TolC share the feature that they are capable of handling drugs with diverse properties (i.e., solvophobic and solvophilic solutes with a wide range of sizes and polyatomic structures) [9]. This feature, which is known as "multidrug efflux," is in marked contrast with, for example, the high selectivity often found in the receptor-ligand binding. The elucidation of the multidrug efflux is also an important target to be tackled. The entropic component of the potential of mean force between a solute and a protein complex is the key factor.

2.3 Entropic Excluded-Volume Effect

As shown in Fig. 2.1a, the presence of a large particle, a solute, in small particles forming the solvent generates a space from which centers of the small particles are excluded (the space occupied by the large particle itself plus the space shown in gray). When the small particles are spheres with diameter d_S and the large particle is a sphere with diameter d_L, the excluded space is a sphere with diameter "$d_S + d_L$". Upon the contact of a pair of large spheres (see Fig. 2.1b), the two

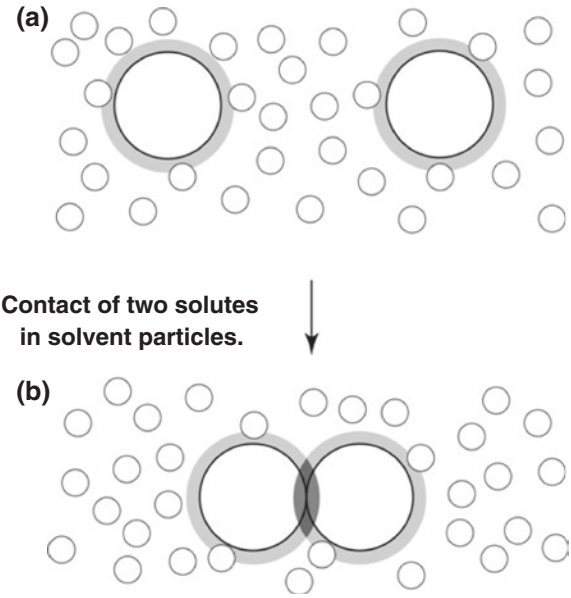

Fig. 2.1 **a** Large spheres, solutes, immersed in small spheres forming the solvent. **b** Contact of a pair of large spheres in small spheres

excluded spaces overlap (the overlapped space is marked in black), and the total volume available to the translational displacement of small spheres increases by the volume of this overlapped space. One might think that the increase leads to a decrease in the system pressure. Upon contact, however, part of the small spheres forming dense layers around the large spheres is released to the bulk, which acts as a factor increasing the system pressure. Consequently, the system pressure does not necessarily decrease: The contact usually occurs almost under isochoric and isobaric conditions. The contact leads to an increase in the number of possible coordinates of centers (i.e., number of accessible translational configurations) of small spheres, except at high pressures. (At high pressures, the release of small spheres forming dense layers around the large spheres to the bulk causes a serious problem: see Sect. 2.9.) Primarily through this effect, the configurational entropy of small spheres increases. An interaction is thus induced between the large spheres, which drives them to contact each other. Since the interaction is induced even when all of the particles are neutral hard spheres with no soft interaction potentials (all of the allowed system configurations share the same energy and the system behavior is purely entropic in origin), it is called "entropic potential" (this is closely discussed in Sect. 2.12).

Hereafter, unless otherwise specified, the small spheres are referred to as "solvent molecules." The entropic effect described above, which is often called *entropic excluded-volume effect*, becomes stronger with an increase in the packing fraction η_S ($\eta_S = \pi\rho_S d_S^3/6$ where ρ_S is the solvent number density) or with a decrease in the solvent diameter d_S. For example, the free-energy decrease occurring when a pair of spherical solutes contact each other is approximately given as

$-1.5k_BT\eta_S(d_L/d_S)$ for $d_L \gg d_S$ (k_B is the Boltzmann constant) when the system pressure is sufficiently low [1]. Water can exist as a dense liquid at ambient temperature and pressure despite its exceptionally small molecular size thanks to the hydrogen bonding [11]. Among the ordinary liquids in nature, the entropic effect becomes the strongest when the solvent is water. Though d_S of neon is almost equal to that of water, it is in gas state at ambient temperature and pressure, resulting in a negligibly small entropic effect. Cyclohexane is in liquid state but its molecular size is considerably larger than that of water, leading to a considerably weaker entropic effect.

2.4 Basic Concept of Entropically Driven Self-assembly Processes

For highly nonspherical solutes, something very interesting happens. Figure 2.2, where the solute shape is cylindrical or disclike, illustrates four different manners of solute contact. Manner 4, the most ordered contact, maximizes the increase in total volume available to the translational displacement of water molecules. That is, water drives the solutes to contact each other in manner 4. Of course, such an ordered contact causes a decrease in the solute entropy, but it brings an increase in water entropy. Unless the solute concentration is extremely low, the water-entropy increase dominates, and the total entropy increases. This is the physical essence of *entropically driven* self-assembly [1, 12].

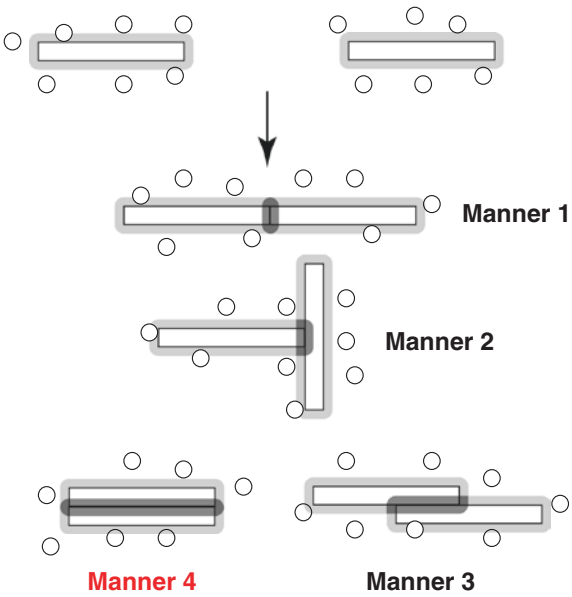

Fig. 2.2 Four typical manners (Manners 1 through 4) of contact of solutes immersed in water. The solute shape is cylindrical or disclike. Manner 4 leads to the largest reduction of the total excluded volume for water molecules

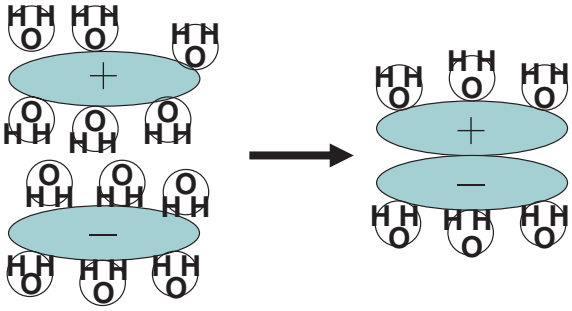

Fig. 2.3 Contact of oppositely (positively and negatively) charged groups of biomolecules in water. Note that an oxygen atom (O) in a water molecule carries a negative partial charge and a hydrogen atom (H) in it carries a positive one. The charges of the groups are screened by water molecules. Moreover, the energy decrease due to a gain of electrostatic attractive interaction between the two groups is accompanied by the energy increase due to a loss of electrostatic attractive interactions between the positively charged group and water oxygen atoms and between the negatively charged group and water hydrogen atoms. Roughly half of the energy increase is canceled out by the energy decrease arising from structure reorganization of the released water [2, 3]: Still, the remaining energy increase is almost as large as the energy decrease mentioned above

It is often claimed that the energy decrease arising from a gain of intramolecular or intermolecular electrostatic attractive interactions for biomolecules drives a biological self-assembly process. However, they accompany an energy increase as explained in Fig. 2.3. We have shown that the decrease and the increase are rather compensating. The increase is often larger, leading to a positive change in enthalpy [2, 3]. A formation of intramolecular or intermolecular hydrogen bonds by biomolecules is accompanied by a break of biomolecule-water hydrogen bonds. The formation and the break are rather compensating or the effect of the latter is often larger. Likewise, a gain of intramolecular or intermolecular van der Waals attractive interactions for biomolecules and a loss of biomolecule-water van der Waals attractive interactions accompanied are rather compensating though the gain is usually larger in this case.

As explained in Sect. 2.8, many of the biological self-assembly processes are driven by a great gain of water entropy which predominates over the conformational-entropy loss of biomolecules. The enthalpy change is often positive for the reasons mentioned above. Hence, $\Delta S > 0$, $\Delta H > 0$, and $|\Delta H| < |T\Delta S|$. This is completely opposite to the most widely accepted view explained in Chap. 1.

2.5 Integral Equation Theory

Our major theoretical tool, the integral equation theory (IET) based on classical statistical mechanics [13], is briefly described here. In this theory, from the system partition function, various correlation functions are defined, and the basic

equations satisfied by these functions are derived. The many-body correlations are approximately taken into account. The average value of a physical quantity is calculated for an infinitely large system and an infinitely large number of system configurations. In the case of bulk solvent of a single component, for example, the temperature, number density, and interaction potential form the input data. Once the basic equations are numerically solved and the correlation functions are obtained, we can calculate the microscopic structure and thermodynamic quantities.

In a molecular solvent such as water, the interaction potential is dependent not only on the distance between centers of molecules but also on their orientations represented by the three Euler angles: The potential is angle dependent. Such a solvent can also be treated, in which case the basic equations must be reduced *mathematically* before the numerical treatment: The theory is referred to as "angle-dependent integral equation theory (ADIET)" [13–15]. The ADIET is combined with a multipolar model for water [14, 15]. In the simplest treatment, a water molecule is modeled as a hard sphere with diameter $d_S = 0.28$ nm in which a point dipole and a point quadrupole of tetrahedral symmetry are embedded. The effect of the molecular polarizability is taken into account using the self-consistent mean field (SCMF) theory [14, 15]. At the SCMF level the many-body induced interactions are reduced to pairwise additive potentials involving an effective dipole moment.

The solvent structure near a solute molecule and thermodynamic quantities of solvation, that is, changes in thermodynamic quantities upon solute insertion into the solvent, can be analyzed by the IET [16, 17]. A thermodynamic quantity of solvation is calculated for a fixed solute structure inserted into a fixed position within the solvent. When the solvent is a simple fluid whose particles interact through radial-symmetric potential, a complex solute molecule with a polyatomic structure (e.g., a protein) can directly be handled by the three-dimensional integral equation theory (3D-IET) [18–20]. When the solvent is water, however, the treatment of the complex solute molecule requires a special approach developed by us (see Sect. 2.6) for avoiding the mathematical complexity and unacceptably long computation time.

2.6 Morphometric Approach for a Complexly Shaped Solute

The ADIET is not directly applicable to a complexly shaped solute like a protein due to the mathematical complexity encountered. Therefore, we developed a judicious treatment referred to as "morphometric approach (MA)" [21, 22]. In arguing the biological self-assembly processes, the most important quantity is the hydration entropy S (i.e., water-entropy loss upon solute insertion into water). An important point is that S is rather insensitive to the solute–water interaction potential

and only the geometric properties of the solute are crucial in calculating S. The idea of the MA is that the solute structure is represented only by the following four geometric measures: the excluded volume (V_{ex}), water-accessible surface area (A), and integrated mean and Gaussian curvatures of water-accessible surface (X and Y). S/k_B is expressed by the linear combination of the four geometric measures, $C_1V_{ex} + C_2A + C_3X + C_4Y$, for any solute. The four coefficients C_1–C_4 are considered independent of the solute geometric properties. Therefore, they can be determined using solutes with the simplest geometries. We calculate S for solutes of neutral hard spheres with various diameters (each solute is isolated): This calculation can be performed by the ADIET. C_1–C_4 are then determined by the least squares fitting applied to the linear combination for spherical solutes. (C_1–C_4 are dependent on the solvent species, temperature, and pressure.) Once C_1–C_4 are determined, S of a protein with a given structure (it is modeled as a set of fused neutral hard spheres accounting for its polyatomic structure on the atomic level) is obtained only if V_{ex}, A, X, and Y are calculated from the diameters and (x, y, z)-coordinates of all of the atoms constructing the protein. The calculation is finished in ~1 s per structure even for a very large protein on a standard workstation. The high speed is quite important because for a protein a number of different structures must usually be considered when an analysis on its structural stability is undertaken. When the solvent is a simple fluid like a Lennard-Jones liquid, S of a protein can directly be calculated using the 3D-IET [18–20]. We have verified for simple-fluid cases that the error in S from the MA is within ±5 %. The ADIET-MA hybrid thus developed has been quite useful to the solution of a variety of important problems related to biological systems.

2.7 Solvent Crowding

It should be noted that the presence of a solvent molecule also generates an excluded volume (EV) for the other solvent molecules, with the result that all of the solvent molecules are entropically correlated. Therefore, the translational freedom of each solvent molecule is restricted by the other solvent molecules in the system, which is referred to as "solvent crowding." The solvent crowding represents the solvent-solvent pair and many-body correlations. The solvent-solvent many-body correlation comprises the solvent-solvent-solvent triplet and higher-order correlations. Upon solute insertion, the solvent crowding becomes more serious. This effect arises from the solute-solvent-solvent triplet and higher-order (i.e., solute-solvent many-body) correlations. We have shown that the biomolecule-water many-body correlations play critical roles [12, 23].

A difference between the solute-solvent pair and many-body correlations can be described as follows [12, 23]. When a solvent molecule contacts a solute as illustrated in Fig. 2.4, an overlap of the EVs generated by the solvent molecule and the solute occurs. The total volume available to *the other solvent molecules* increases by this overlapped volume. Though the translational freedom of solvent

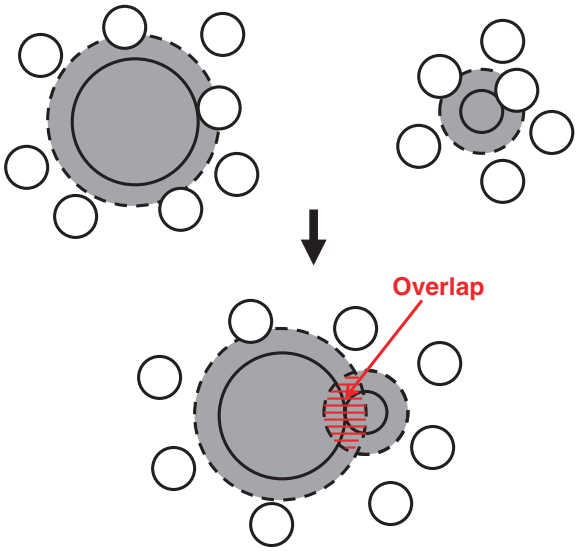

Fig. 2.4 Contact of a solvent molecule with a solute. The excluded volumes generated by the solvent molecule and the solute overlap. The total volume available to the other solvent molecules increases by this overlapped volume

molecules in contact with the solute is decreased (effect 1), that of the other solvent molecules is increased (effect 2). Effects 1 and 2 originate from the solute-solvent pair and many-body correlations, respectively.

2.8 Protein Folding

We have shown that even in the complete absence of potential energies among the atoms in a protein-aqueous solution system, there is a physical factor which strongly favors the folded state of the protein: The factor is the translational displacement of water molecules in the system [24]. A simple illustration is shown in Fig. 2.5 [25]. It can be argued for a solute with cylindrical shape generating an EV that the formation of helical structure by a cylinder or the lateral contact of cylinders leads to a reduction of the EV. This argument can be applied to the backbone of a protein. The α-helix construction accompanies a formation of the helical structure by a portion of the backbone (see Fig. 2.5a). A lateral contact of portions of the backbone occurs in the β-sheet construction (see Fig. 2.5b). Each of these constructions leads to a reduction of the EV followed by a corresponding gain of water entropy. When the α-helix or the β-sheet is formed, not only a water-entropy gain occurs but also the energetically unfavorable break of hydrogen bonds *with water molecules* is compensated with the formation of intramolecular hydrogen bonds. Hence, these secondary structures (α-helix and β-sheet) are very advantageous units to be formed as much as possible in protein folding [25]: This is why they frequently appear in the native structure. The packing of side chains is also crucially important. The presence of a side chain generates an EV which the

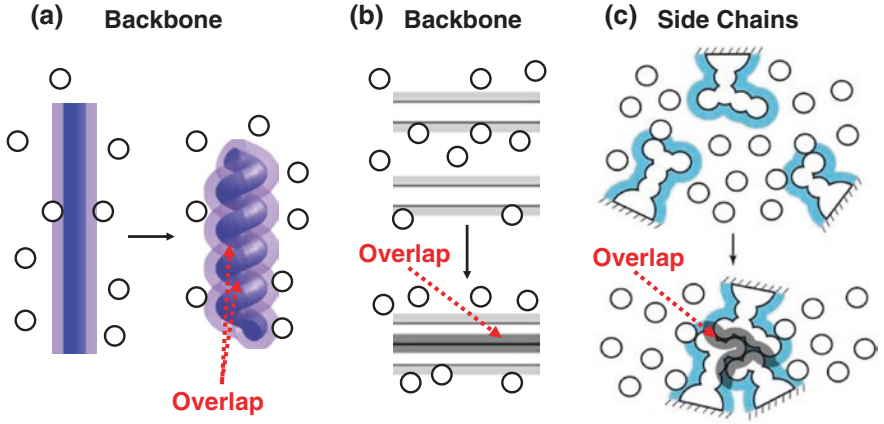

Fig. 2.5 **a** Formation of helical structure by a portion of the backbone. **b** Lateral contact of portions of the backbone. **c** Close packing of side chains. Excluded volumes overlap [overlap of an excluded volume occurs in (**a**)], and the total volume available to the translational displacement of water molecules increases by the overlapped volume

centers of water molecules cannot enter. When the side chains are closely packed (or contact one another) as illustrated in Fig. 2.5c, the EVs overlap with the result of a large gain of water entropy.

The factors in favor of protein folding are the gain of water entropy explained above, decrease in protein intramolecular (conformational) energy, and decrease in water–water interaction energy (i.e., structure reorganization energy of the water near the protein surface). The factors opposing protein folding are the loss of protein intramolecular entropy and the increase in protein–water interaction energy. The decrease and the increase in energy are rather compensating or the latter is often larger [26]. It has been shown in a recent study using a novel experimental technique that apoplastocyanin (apoPC) folding at 298 K accompanies a large gain of system entropy [26], which manifests that the water-entropy gain is much larger than the conformational-entropy loss. (The system-volume change upon apoPC folding measured is almost zero, and the folding is both isochoric and isobaric. See Sect. 2.3.) According to the usual view, which considers only the water in the close vicinity of the protein surface, the water adjacent to nonpolar groups is entropically unstable, and protein folding is promoted by the release of such unfavorable water to the bulk through the burial of nonpolar groups. We have shown that the entropic gain originating from this view is certainly present but too small to elucidate the very large water-entropy gain. Upon protein folding, the water crowding in the bulk is largely reduced by a decrease in the EV generated by the protein. This reduction is a principal contributor to the very large water-entropy gain [23]. (See Sect. 4.7 for the correct physical interpretation of the hydrophobic effect.) The entropic gain is *quantitatively* reproducible by our theoretical method wherein the ADIET-MA hybrid applied to the multipolar water model is employed.

Water possesses not only the translational entropy but also the orientational (rotational) entropy. The water-entropy change upon protein folding/unfolding can be decomposed into the translational and orientational contributions [17]. We have shown that the translational contribution predominates over the orientational one. For instance, the translational and orientational contributions to the water-entropy gain upon apoPC folding are ~95 and ~5 %, respectively [26]. The translational contribution can be decomposed into the EV-dependent term and the term which is dependent on the water-accessible surface area (ASA) and surface curvature. Each term can further be decomposed into the protein-water pair and many-body correlation components [23]. We have shown that the many-body correlation component predominates over the pair one. The many-body correlation component of the EV-dependent term, which corresponds to the water crowding, is an important factor in the elucidation of pressure and cold denaturating of a protein.

2.9 Pressure and Cold Denaturating of a Protein

It is experimentally known that at high pressures a protein is denatured. The pressure-denatured state is characterized by the penetration of water molecules into the protein interior. Its EV is slightly larger than that of the native structure, but its ASA is much larger [23, 27]. A pressure-denatured structure is therefore referred to as "swelling structure." This pressure denaturation can beautifully be elucidated by our theory wherein the water-entropy effect is treated as the key factor [12, 23, 27]. Let us return to Sect. 2.7. The number of water molecules (i.e., density structure of water in the close vicinity of the protein surface) is determined by the interplay of the two opposing effects, effects 1 and 2. At low and high pressures, respectively, the water crowding is moderate and serious. At low pressures, effect 2 is relatively less important, with the result that the number of water molecules in contact with the protein surface is made sufficiently small due to effect 1. At high pressures, by contrast, effect 2 becomes relatively more important, and considerably many water molecules are driven to contact the protein surface. Since the protein possesses a flexible, polyatomic structure, its structure is to be changed to the one with a much larger ASA. At the same time, however, its EV must be kept sufficiently small for preventing a serious increase in the water crowding. To meet these requirements, water penetrates into the protein interior, leading to quite a large number of water molecules contacting the protein surface with the compactness of the structure retained. Although the translational freedom of water molecules penetrating into the protein interior is decreased, that of water molecules well outside the protein surface is increased. The increase is larger than the decrease at high pressures, leading to a positive net change in water entropy upon the denaturation.

It is interesting that at low temperatures a protein is denatured to a state which is significantly more extended than the pressure-denatured one [28]. The water crowding, which is the primary driving force in protein folding, becomes weaker

when the temperature is lowered. Consequently, the net power of factors in favor of protein folding (the water-entropy gain, decrease in protein intramolecular energy, and decrease in water-water interaction energy) yields to that of factors opposing the folding (the loss of protein intramolecular entropy and the increase in protein-water interaction energy) [12, 23]. The weakening of water crowding is ascribed to the enhanced local association of water molecules in the bulk due to stronger hydrogen bonding, giving rise to more inhomogeneity followed by the formation of more void space: Water can then accommodate a protein possessing large EV with less difficulty [29]. Thus, the temperature dependence of the water crowding, which plays pivotal roles in cold denaturation of a protein, is substantially influenced by the hydrogen bonds.

2.10 Modeling Water as Neutral Hard Spheres with no Soft Interaction Potentials

The solvent-entropy effect emphasized in this book can be taken into account only by treating the solvent as an ensemble of particles with sizes. Hereafter, neutral hard spheres are referred to simply as "hard spheres": Likewise, "hard-sphere model" in this book implies that there are no soft interaction potentials considered. Though the hard-sphere model is the most fundamental one in liquid state physics, it is not capable of reproducing the unique properties of water. What about the solvation properties of a solute? We have calculated the hydration free energy μ, entropy S, and energy U under isochoric condition for a spherical solute using the ADIET applied to the multipolar model water mentioned above [14–17, 30]. The hydration free energy, for example, is the free-energy change upon the insertion of a solute into pure water. The solute diameter is set at the molecular diameter of water 0.28 nm. For the hard-sphere solute with zero charge, the calculated values are $\mu = 5.95k_BT$, $S = -9.22k_B$, and $U = -3.27k_BT$ ($\mu = U - TS$). (The solute insertion enhances the restriction of translational freedom of water molecules in the system, which is the major physical origin of "hydrophobicity.") When the point charge $-0.5e$ (e is the electronic charge) is embedded at its center, the calculated values become $\mu = -32.32k_BT$, $S = -10.11k_B$, and $U = -42.43k_BT$. Thus, S is fairly insensitive to the solute-water interaction potential while μ and U are largely influenced by it. The insensitivity implies that the contribution from the solvent near the solute to S is considerably small. Even when the solvent is replaced by hard spheres whose number density and diameter are those of water, the result is the following: $\mu = 9.64k_BT$ and $S = -9.64k_B$ ($U = 0$). Thus, the solvation entropy can approximately be evaluated even by modeling water as hard spheres.

Water possesses not only the translational entropy (TE) but also the orientational (rotational) entropy (OE). The OE is larger than the TE in bulk water [31], whereas the TE contribution predominates over the OE one in the solute hydration (i.e., water-entropy change upon solute insertion) [17, 26]. This is because upon solute insertion the reduction of orientational freedom occurs only for the water

near the solute but that of translational freedom reaches the whole water in the system. As a consequence, in many cases the water-entropy effect can be analyzed by modeling water as neutral hard spheres with no soft interaction potentials as long as the packing fraction and molecular diameter are set at those of water (i.e., the results from the hard-sphere model for water are at least qualitatively correct). An exception is the case where the temperature dependence of the effect plays important roles. For example, the increase in solubility of methane observed at low temperatures and cold denaturation of a protein cannot be elucidated by the hard-sphere model for water [23, 29]. The temperature dependence of the effect is ascribed to the interplay of strongly attractive interaction (i.e., hydrogen bonding) and exceptionally small molecular size of water.

2.11 Roles of Potential of Mean Force in Ordering Processes

We have shown that in the unidirectional movement of myosin head S1 along filamentous actin (F-actin) [4] or in the insertion and release of a solute into and from a protein complex [7–10], the potential of mean force (PMF) formed by water between F-actin and S1 or the protein complex and the solute plays essential roles. The PMF is defined for a solute pair (e.g., S1/F-actin or protein complex/solute pair) as "free energy of water for a fixed configuration of the pair" minus "that for the configuration where the pair is infinitely separated." The location of F-actin or the protein complex is considered to be fixed, and the PMF is treated as a function of the position of S1 or the solute. We can take the view that S1 or the solute feels a potential field represented by the PMF near F-actin or the protein complex. In general, a solute feels no potential field in bulk solvent. However, it feels a potential in the solvent confined by another solute. A spatial distribution, in which the potential becomes largely positive and largely negative with a periodicity of the solvent diameter d_S, is formed as described in Sects. 2.12, 3.3 and 3.4.

We focus on a chaperonin-protein pair (a chaperonin is the protein complex and a protein is the solute) hereafter and the chaperonin is referred to as "vessel." Within the vessel, the PMF becomes largely positive and largely negative with a periodicity of the molecular diameter of water, 0.28 nm [8]. This is because the spatial distribution of the PMF cannot be described by the overlap of EVs generated by the vessel and the solute alone [1, 20, 32]. It is influenced by the density structure of water within the domain confined by the vessel-solute pair (see Sect. 2.12). The PMF is calculated on the assumption that water molecules are always in equilibrium with each configuration of the vessel-protein pair. This assumption is justified because the time scale of the water-structure steadying is orders of magnitude shorter than that of the protein movement [33]. The 3D-IET [18–20] is employed to calculate the spatial distribution of the PMF. It gives the spatial distribution of the PMF in a single calculation, whereas a molecular dynamics (MD) simulation gives only the value of the PMF on a single position.

2.12 Entropic Potential or Force

The PMF Φ can be decomposed into energetic and entropic components: $\Phi = \Phi_E - T\Phi_S$. The entropic component $-T\Phi_S$, which is referred to as "entropic potential" hereafter, often plays essential roles in the ordering processes. When two large hard bodies immersed in small hard spheres forming the solvent are considered and no soft interaction potentials are present, there is only the entropic component: $\Phi = -T\Phi_S$. Here, we consider the entropic potential induced between large particles (solutes) or between a large particle and a planar wall (a surface). The presence of the wall also generates an EV for small particles forming the solvent. It is assumed that the small and large particles are hard spheres and the wall is a hard wall with no soft interaction potentials. In the description of the entropic potential, an argument on the basis of the overlap of the EVs alone is valid only when the number density of small spheres ρ_S is sufficiently low. In cases where ρ_S is high, due to the microscopic structure of small spheres formed within the domain confined by two large spheres or by a large sphere and the wall, the entropic potential oscillates (i.e., attractive and repulsive regions appear alternately) with the periodicity d_S [1, 20, 32]. This effect can be accounted for only by employing elaborate statistical-mechanical theories such as the integral equation theory.

Figure 2.6 shows an example of the entropic potential induced between a large sphere and a planar wall immersed in small spheres, $\Phi_{Wall}(h)$ (h is the nearest distance between large sphere and wall surfaces). The entropic potential between large spheres exhibits qualitatively the same behavior. $\Phi_{Wall}(h_0)$ represents the free energy of small spheres in the case of $h = h_0$ *relative to* that in the case of $h \to \infty$. The entropic force, $F_{Wall}(h) = -d\Phi_{Wall}(h)/dh$, is shown in Fig. 2.7. $F_{Wall}(h_0)$ represents

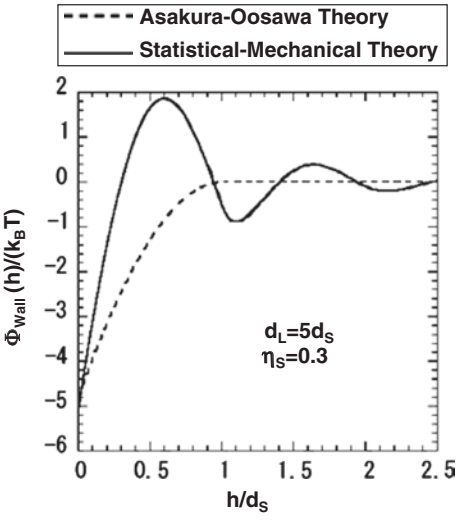

Fig. 2.6 Entropic potential Φ_{Wall} induced between a large sphere and a planar wall immersed in small spheres. T, k_B, h, d_L, and d_S denote the absolute temperature, Boltzmann constant, surface separation, diameter of the large sphere, and diameter of the small spheres, respectively

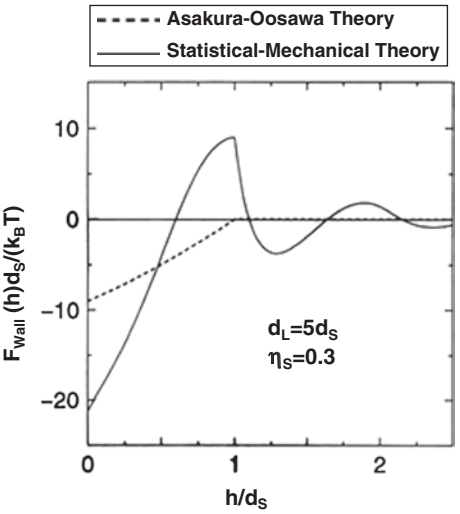

Fig. 2.7 Entropic force F_{Wall} induced between a large sphere and a planar wall immersed in small spheres. T, k_{B}, h, d_{L}, and d_{S} denote the absolute temperature, Boltzmann constant, surface separation, diameter of the large sphere, and diameter of the small spheres, respectively. Also see Fig. 2.6: $F_{\mathrm{Wall}}(h) = -d\Phi_{\mathrm{Wall}}(h)/dh$

the force induced between the large sphere and the wall averaged over all possible configurations of the small spheres with h fixed at h_0. In Figs. 2.6 and 2.7, two curves calculated using the Asakura–Oosawa (AO) theory [34, 35] and a statistical-mechanical theory (e.g., the IET) are compared. (In the original AO theory, large bodies immersed in small particles were considered. In the present case, they correspond to solutes immersed in the solvent). In the AO theory, only the EV term of the solute-solvent pair correlation is considered: See Sect. 2.7. Further, the potential or force is evaluated using the overlap of EVs alone. Hence, as observed in Fig. 2.6, no force is induced between a large sphere and the wall as long as there is no overlap of the two EVs generated. The overlap occurs only for $h < d_{\mathrm{S}}$ and a force is induced to increase the overlapped volume. The force is always attractive and its strength increases monotonically with decreasing h. By contrast, the *exact* force is oscillatory with a periodicity of d_S and longer ranged [1, 20, 32]. This behavior is ascribed to the microscopic structure of small spheres formed within the domain confined by a large sphere and the wall. The AO theory neglects the microscopic structure.

We note that the two curves in Fig. 2.6 share almost the same value of the entropic potential at contact $\Phi_{\mathrm{Wall}}(0)$. $\Phi_{\mathrm{Wall}}(0)$ is the free-energy decrease of small spheres occurring when the large sphere contacts the wall. In the simple cases where a large sphere contacts another large sphere or a planar wall, fortuitous cancelation of errors occurs in the calculation of $\Phi_{\mathrm{Wall}}(0)$ using the AO theory [20]. Only in the solid curve in Fig. 2.6, however, there exists a free-energy barrier for the large sphere to overcome to contact the wall. If the barrier is much higher than $k_{\mathrm{B}}T$, the large sphere cannot come in contact with the wall. Such a barrier often plays important roles: A good example is found in the case of molecular recognition described by a lock-key mechanism [20]. The high size selectivity, "only the key that exactly fits the lock can accomplish the binding, and smaller keys as well as larger keys cannot bind to the lock," is explainable only in the presence of

the barrier. Interestingly, such a high selectivity can be reproduced by the entropic effect alone. Here, it is worthwhile to remark the following: The AO theory fails to correctly estimate the free-energy decrease of small spheres upon contact of two solutes when the solute shapes are complex [20]. (If the AO theory is applied to a protein folding problem, for example, it excessively underestimates the water-entropy gain and fails to elucidate the temperature and pressure dependences of the water-entropy effect because it accounts for only the EV-dependent term of the protein-water pair correlation component. As a striking example, the AO theory predicts that the native structure is increasingly more stabilized as the pressure becomes higher.)

The entropic potential is quite strong when the solvent is water. One might think that a strong electrostatic interaction between groups with significantly large charges surpasses the entropic potential. We emphasize that the charges are screened by water molecules and counter ions. Though an electrostatic attractive or repulsive interaction between charged groups of a biomolecule or biomolecules is quite strong and long ranged in vacuum, it becomes about two orders of magnitude weaker and much shorter ranged in aqueous solution (~0.15 M-NaCl solution in biological systems) due to the screening effects [36]. Consequently, the entropic potential plays essential roles.

References

1. M. Kinoshita, Front. Biosci. **14**, 3419 (2009)
2. T. Hayashi, H. Oshima, T. Mashima, T. Nagata, M. Katahira, M. Kinoshita, Nucleic Acids Res. **42**, 6861 (2014)
3. T. Hayashi, H. Oshima, S. Yasuda, M. Kinoshita, J. Phys. Chem. B **119**, 14120 (2015)
4. K. Amano, T. Yoshidome, M. Iwaki, M. Suzuki, M. Kinoshita, J. Chem. Phys. **133**, 045103 (2010)
5. T. Yoshidome, Y. Ito, M. Ikeguchi, M. Kinoshita, J. Am. Chem. Soc. **133**, 4030 (2011)
6. T. Yoshidome, Y. Ito, N. Matubayasi, M. Ikeguchi, M. Kinoshita, J. Chem. Phys. **137**, 035102 (2012)
7. K. Hollenstein, R.J.P. Dawson, K.P. Locher, Curr. Opin. Struct. Biol. **17**, 412 (2007)
8. K. Amano, H. Oshima, M. Kinoshita, J. Chem. Phys. **135**, 185101 (2011)
9. H. Mishima, H. Oshima, S. Yasuda, K. Amano, M. Kinoshita, J. Chem. Phys. **139**, 205102 (2013)
10. H. Mishima, H. Oshima, S. Yasuda, M. Kinoshita, J. Phys. Chem. B **119**, 3423 (2015)
11. K. Soda, J. Phys. Soc. Jpn. **62**, 1782 (1993)
12. M. Kinoshita, Biophys. Rev. **5**, 283 (2013)
13. J.-P. Hansen, L.R. McDonald, *Theory of Simple Liquids*, 3rd edn. (Academic, London, 2006)
14. P.G. Kusalik, G.N. Patey, J. Chem. Phys. **88**, 7715 (1988)
15. P.G. Kusalik, G.N. Patey, Mol. Phys. **65**, 1105 (1988)
16. N.M. Cann, G.N. Patey, J. Chem. Phys. **106**, 8165 (1997)
17. M. Kinoshita, J. Chem. Phys. **128**, 024507 (2008)
18. D. Beglov, B. Roux, J. Chem. Phys. **103**, 360 (1995)
19. M. Ikeguchi, J. Doi, J. Chem. Phys. **103**, 5011 (1995)
20. M. Kinoshita, J. Chem. Phys. **116**, 3493 (2002)
21. P.M. König, R. Roth, K.R. Mecke, Phys. Rev. Lett. **93**, 160601 (2004)

22. R. Roth, Y. Harano, M. Kinoshita, Phys. Rev. Lett. **97**, 078101 (2006)
23. H. Oshima, M. Kinoshita, J. Chem. Phys. **142**, 145103 (2015)
24. Y. Harano, M. Kinoshita, Biophys. J. **89**, 2701 (2005)
25. S. Yasuda, T. Yoshidome, H. Oshima, R. Kodama, Y. Harano, M. Kinoshita, J. Chem. Phys. **132**, 065105 (2010)
26. T. Yoshidome, M. Kinoshita, S. Hirota, N. Baden, M. Terazima, J. Chem. Phys. **128**, 225104 (2008)
27. Y. Harano, T. Yoshidome, M. Kinoshita, J. Chem. Phys. **129**, 145103 (2008)
28. H. Oshima, T. Yoshidome, K. Amano, M. Kinoshita, J. Chem. Phys. **131**, 205102 (2009)
29. T. Yoshidome, M. Kinoshita, Phys. Chem. Chem. Phys. **14**, 14554 (2012)
30. M. Kinoshita, S. Iba, K. Kuwamoto, M. Harada, J. Chem. Phys. **105**, 7177 (1996)
31. T. Lazaridis, M. Karplus, J. Chem. Phys. **105**, 4294 (1996)
32. M. Kinoshita, Chem. Eng. Sci. **61**, 2150 (2006)
33. F. Jülicher, A. Ajdari, J. Prost, Rev. Mod. Phys. **69**, 1269 (1997)
34. S. Asakura, F. Oosawa, J. Chem. Phys. **22**, 1255 (1954)
35. S. Asakura, F. Oosawa, J. Polym. Sci. **33**, 183 (1958)
36. M. Kinoshita, Y. Harano, Bull. Chem. Soc. Jpn **78**, 1431 (2005)

Chapter 3
Molecular Machines

Abstract The ATP hydrolysis cycle is utilized in such processes as the unidirectional movement of myosin along F-actin, assistance in protein folding performed by a chaperonin, transport of diverse substrates across the membrane by an ABC transporter, and rotation of the central subunit within F_1-ATPase. On the other hand, the proton motive force is utilized in the functional rotation of the multidrug efflux transporter AcrB. In this chapter, we elucidate the mechanism of these ordering processes. We also argue how the processes are coupled with the ATP hydrolysis cycle or the proton motive force. Like in the self-assembly processes, the key factor is the entropic effect originating from the translational displacement of water molecules in the system.

Keywords ATP · Myosin · F-actin · Chaperonin · Transporter

3.1 Proteins and Protein Complexes Utilizing ATP Hydrolysis Cycle and Proton Motive Force

There are proteins or protein complexes sharing the feature that they function by utilizing the cycle comprising binding of ATP to a receptor within a protein or protein complex, hydrolysis of ATP into ADP+Pi within the receptor, and dissociation of ADP and Pi from the receptor. Though the receptor has lower affinity with ADP than with ATP, the binding free energy takes a large, negative value for ADP as well as for ATP. Here, the binding free energy is defined as the free-energy change which would occur when the ligand-receptor binding is completed under the condition where the receptor and the ligand (ATP or ADP) are immersed in aqueous solution at infinite dilution. Actomyosin [1], chaperonins [2], F_1-ATPase [3, 4], and ABC transporters [5] function in the environment that the ATP and ADP concentrations are sufficiently high and sufficiently low, respectively. Of course, the binding of ATP leads to a decrease in the system free energy (SFE). When the ADP concentration is sufficiently low, dissociation of ADP is promoted due to the effect of entropy of mixing: The dissociation of ADP also leads to a

M. Kinoshita, *Mechanism of Functional Expression of the Molecular Machines*,
SpringerBriefs in Molecular Science, DOI 10.1007/978-981-10-1486-4_3

decrease in the SFE. The hydrolysis of ATP within the receptor is followed by a small decrease in the SFE. It is not definite if the Pi-receptor binding free energy is negative or positive, but dissociation of Pi occurs when the Pi concentration is sufficiently low. Thus, any of the ATP binding, hydrolysis, and dissociation of ADP or Pi leads to a decrease in the SFE and unavoidably occurs. The cycle is repeated, and in each cycle a protein or protein complex expresses high function. Good examples are the unidirectional movement of a linear-motor protein along a filament, transport of diverse substrates across the membrane by an ABC transporter, and directed rotation of the central subunit within F_1-ATPase.

There are also proteins or protein complexes which function by utilizing the proton motive force [6]. They interact with two aqueous solutions where the proton concentrations are higher and lower, respectively. The two solutions are referred to as higher-concentration and lower-concentration sides, respectively. When a proton-binding site with no proton bound within a protein or protein complex is exposed to the higher-concentration side, proton binding occurs because it leads to a decrease in the SFE (the site-proton binding free energy is negative). On the other hand, when a proton-binding site with a proton bound is exposed to the lower-concentration side, proton dissociation occurs because it also leads to a decrease in the SFE due to the effect of entropy of mixing (see Supporting Information of one of our earlier publications [6] for more details of this effect). As a result, a proton is transferred from the higher-concentration side to the lower-concentration one, and the transfer unavoidably occurs. The proton-transfer cycle is repeated, and by each transfer a protein or protein complex expresses high function (e.g., functional rotation of AcrB considered in Sect. 3.6).

It is important to outline the whole ATP hydrolysis or proton-transfer cycle. Statistical thermodynamics is best suited to such an outlining analysis. In this book, we are not very interested in a detailed investigation on a particular aspect or an elemental process in the cycle which is usually performed by an MD simulation.

3.2 Unidirectional Movement of Myosin Head (S1) Along F-Actin

The linear-motor proteins such as kinesins [7], dyneins [8], and myosins [9] share the following common characteristics: They move in one direction along the filaments, similar in function to railway tracks, which possess periodic structures; and they repeat the cycle comprising binding of ATP to the motor domain (i.e., head) of the protein, hydrolysis of ATP into ADP+Pi, and dissociation of Pi and ADP [10, 11]. Many of them have two-headed structures, but it has been found that even a single-headed kinesin [12] or a single myosin head [13, 14] [i.e., myosin subfragment 1 (S1)] exhibits unidirectional movement. Hence, the fundamental physics can be extracted by means of studies for a single linear-motor protein head.

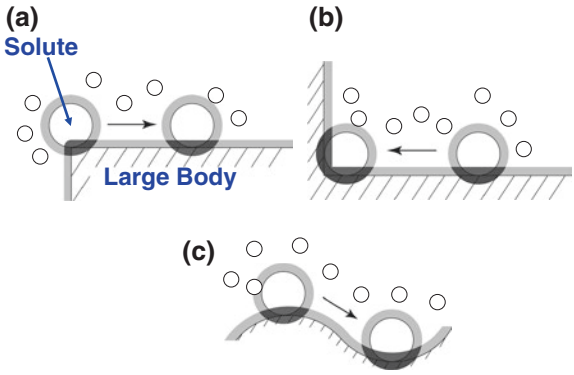

Fig. 3.1 Entropic force (or potential) acting on a solute sitting on a large body in solvent. The solute is locally repelled from a step edge (**a**), attracted to a corner (**b**), and moved from a convex surface to a concave one (**c**)

Let us consider a solute sitting on a large body (see Fig. 3.1). The solute and the large body generate the EVs for water molecules. The solute tends to be moved so that the overlapped volume marked in black can increase and the translational entropy of water can increase. For example, the solute is repelled from a step edge, trapped at a corner, and transferred from a convex surface to a concave one. A potential field is thus formed for the solute *along* the large body. As discussed in Sect. 2.12, the field is rather complicated and to be calculated using a statistical-mechanical theory such as the 3D-IET [15–17]. The field is strongly dependent on the geometric properties of the solute as well. In other words, the solute movement can be controlled by adjusting, for example, the solute geometry. We have recently suggested a new concept that the unidirectional movement of the linear-motor proteins is controlled in this manner primarily through the entropic effect originating from the translational displacement of water molecules [1].

3.2.1 Summary of Experimental Observations

Myosin, a typical linear-motor protein, moves along F-actin possessing a double helical structure formed by two sets of connected G-actin molecules. It is known that myosin head S1, whose release from F-actin is prevented in an experiment, achieves unidirectional movement [13, 14]. Our theoretical consideration is focused on this experiment. On the basis of experimentally available information [10, 11, 13, 14, 18, 19], it is inferred that the following cycle is repeated (see Fig. 3.2): (1) S1 is strongly bound to a rigor binding site (RBS) of F-actin in the absence of ATP or ADP+Pi binding to S1; (2) S1 can be bound to F-actin only weakly upon ATP binding to S1 [18, 19], and it makes directed movement by a biased Brownian motion; (3) the hydrolysis of ATP into ADP+Pi occurs in the course of the Brownian motion; (4) after Pi dissociates, S1 is bound to the next RBS of F-actin with moderate strength; and (5) after ADP dissociates, S1 is strongly bound to this RBS. The distance between two adjacent RBSs is

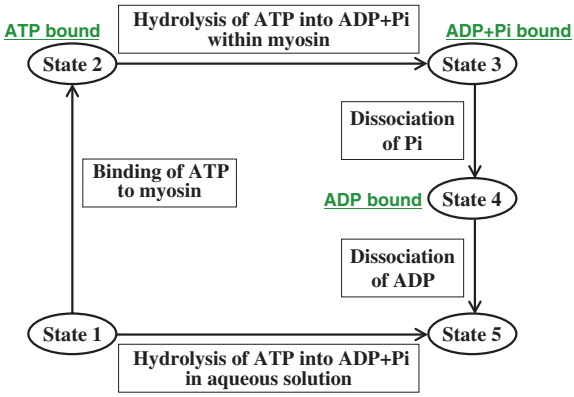

Fig. 3.2 One cycle of ATP hydrolysis comprising state 1→state 2→state 3→state 4→state 5. One APT molecule is hydrolyzed. The hydrolysis of ATP into ADP+Pi in aqueous solution, $ATP + H_2O \rightarrow ADP + Pi + H^+$, accompanies a free-energy decrease of F_H. Myosin possesses geometry 1 in states 1, 4, and 5 and geometry 2 in states 2 and 3 (see the text)

approximately equal to the size of a G-actin molecule. In Step (2), S1 could be released from F-actin but the release is prevented in the experiment [16, 17] (see Sect. 3.2.4 for more details).

3.2.2 Model and Theory

Our major concern is to analyze the spatial distribution of the entropic potential between S1 and F-actin immersed in water by accounting for only overall shapes (not detailed polyatomic structures) of S1 and F-actin as their geometric properties. The analysis is made using the 3D-IET [15–17]. Probably, the geometric properties of myosin in states 1 through 5 shown in Fig. 3.2 are all different. It is experimentally known, however, that myosin with the ATP or ADP+Pi binding in states 2 and 3 has a cleft near the myosin/F-actin interface and that this cleft is closed in myosin without the binding in states 1, 4, and 5 [20, 21]. (When ATP binds to myosin, tight packing of myosin and ATP occurs and the myosin structure undergoes a large change. As a result, the packing of myosin and F-actin is inevitably loosened. The tight packing should be more important than the loosening for increasing the water entropy.) We assume as an approximation that myosin takes only two distinct geometries: one of them is in states 2 and 3 and the other is in states 1, 4, and 5. With the cleft formed, the geometry of myosin becomes more asymmetrical with respect to the y-axis (see Fig. 3.3). We model S1 in states 1, 4, and 5 as a large hard sphere with diameter d_B (geometry 1) and S1 in states 2 and 3 as a large hard sphere with diameter d_B possessing a cleft on the S1/F-actin interface (geometry 2). Geometries 1 and 2 are symmetrical and asymmetrical with respect to the y-axis, respectively.

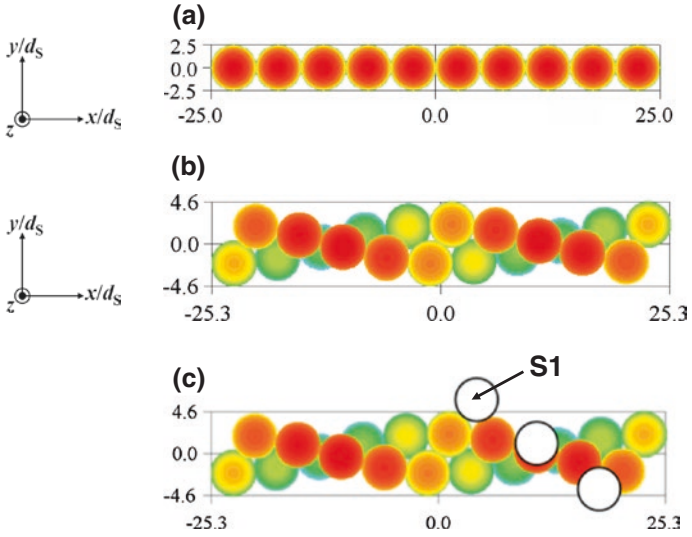

Fig. 3.3 **a** Model I of the filament: one-dimensionally connected large hard spheres. **b** Model II of the filament: double helical structure formed by two sets of connected large hard spheres. The position of an element sphere becomes farther from us as the color approaches *blue*, and the position becomes closer to us as the color approaches *red*. **c** Movement of S1 along the trajectory in harmony with the helical structure

We test two models of F-actin [1]: One-dimensionally connected large hard spheres (model I; Fig. 3.3a) and double helical structure formed by two sets of connected large hard spheres (model II; Fig. 3.3b). The diameter of the large hard spheres is d_G. The solvent is modeled as neutral hard spheres with diameter d_S. In the analysis, d_B and d_G are set at $5d_S$. The numbers of the large hard spheres in models I and II is 20. We have found that S1 can rotate around the x-axis in model I, while S1 cannot in model II due to the spatial distribution of the entropic potential [1]. The focus is placed on the entropic potential along x-axis direction in model I and along the trajectory in harmony with the helical structure illustrated in Fig. 3.3c. If the rotation in model I mentioned above is not allowed, the physical pictures of the unidirectional movement obtained from the two models are essentially the same. The bulk-solvent density ρ_S and d_S are set at those of water under the normal condition: $\rho_S {d_S}^3 = 0.7317$ ($d_S = 0.28$ nm).

3.2.3 Summary of Theoretical Results

We discuss the entropic potential field felt by S1 on F-actin along x-axis direction. Our findings [1] can be summarized as follows. S1 with geometry 1 feels the field looking like the black curve shown in Fig. 3.4a. The curve is symmetrical

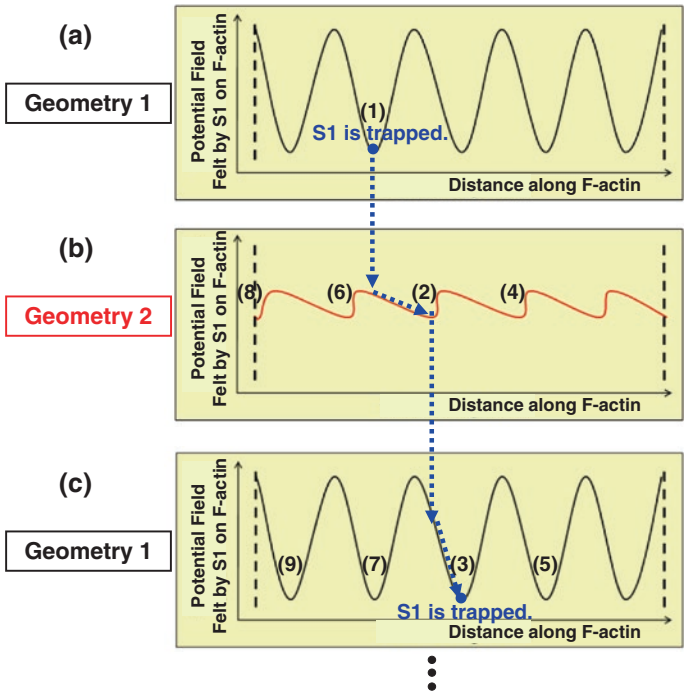

Fig. 3.4 Our physical picture of directed movement of S1 along F-actin. **a**, **c** Potential field felt by S1 with geometry 1 on F-actin. **b** Potential field felt by S1 with geometry 2 on F-actin. The movement of S1 is controlled by adjusting the S1 geometry (a change in the S1 geometry leads to that in the potential field felt by S1): The adjustment is performed by the ATP hydrolysis cycle

with respect to the *y*-axis, its amplitudes are considerably large, there are sites with sharply deep potential minima, and the distance between adjacent sites is ~d_G. S1 is trapped on one of these sites (binding sites): S1 can hardly move. It is interesting that such RBSs are generated through a purely entropic effect. On the other hand, S1 with geometry 2 feels the field looking like the red curve shown in Fig. 3.4b. The curve is asymmetrical with respect to the *y*-axis and its amplitudes are much smaller. The asymmetry arises from the geometrical asymmetry of S1. The cleft near the S1/F-actin interface is responsible for the much smaller amplitudes. Due to the cleft, the decrease in the total EV for water molecules upon the contact of myosin to F-actin becomes smaller, leading to smaller differences between the potential minimum and maximum.

3.2.4 Physical Picture of the Unidirectional Movement

Based on the results from not only our theoretical calculations but also the experimental observations summarized above, we have proposed a physical picture of

the unidirectional movement of S1 along F-actin, which is illustrated in Fig. 3.4. Due to the ATP hydrolysis cycle, S1 is forced to take basically two different geometries (geometries 1 and 2), and the geometry of S1 undergoes repeated switches from one of them to the other. The unidirectional movement is realized by the following three principal steps [1]:

Step 1. S1 without any of ATP, ADP, and Pi bound to it, which possesses geometry 1, is trapped on an RBS (1) in Fig. 3.4a: S1 can hardly move

Step 2. The geometry of S1 changes to geometry 2 upon the ATP binding, which leads to the change in the potential field from the black curve to the red one shown in Fig. 3.4b. (The ATP binding to S1 occurs because the system free energy (SFE) decreases by the binding. After the binding, S1 changes its structure so that the SFE can be minimized.) Along the negative slope of the red curve, S1 moves to a new location with the local potential minimum (2) in Fig. 3.4b. The hydrolysis of ATP occurs during this step

Step 3. The dissociation of Pi occurs. Geometry 1 is recovered and the potential field returns to the black curve (see Fig. 3.4c). Along the negative slope of the black curve, S1 moves to the next RBS (3) in Fig. 3.4c and get trapped on it. (The dissociation of ADP occurs before the ATP binding to S1.)

By these three steps, S1 moves in the right direction, (1)→(2)→(3) (see Fig. 3.4). The sufficiently small amplitudes of the red curve allow a biased Brownian motion of S1, and it sometimes exhibits different movements: It moves forward to a farther location with the local potential minimum (e.g., (1)→(2)→(4)→(5)), it makes essentially no movement ((1)→(6)→(7)), or it moves even backward ((1)→(6)→(8)→(9)). However, the most probable route should be (1)→(2)→(3). Thus, the unidirectional movement of S1 is realized by repeated switches from one of the potential fields to the other. We emphasize the following: The time during which S1 is feeling the potential of red curve must be quite short; otherwise, the movement of S1 will no more be unidirectional even when the potential of red curve possesses the asymmetry.

Here, aqueous solution comprising water molecules, ATP, Pi, and ADP is referred to as the solvent. An entropic potential of the black curve represents "the free energy of the solvent in the case where S1 without the ATP or ADP + Pi binding is on a location of F-actin" *relative to* "the free energy of the solvent in the case where S1 without the ATP or ADP + Pi binding is infinitely separated from F-actin." Likewise, an entropic potential of the red curve represents "the free energy of the solvent in the case where S1 with the ATP or ADP + Pi binding is on a location of F-actin" *relative to* "the free energy of the solvent in the case where S1 with the ATP or ADP + Pi binding is infinitely separated from F-actin." We emphasize that the black and red curves have different reference values of the solvent free energy [1]: For example, the reference value in the red curve in Fig. 3.4a is lower than that in the black curve in Fig. 3.4b by the free-energy change upon the ATP binding. Further, the free energy of the solvent exhibits a small but significant decrease in each of the switches from one of the black

and red curves to the other. When S1 moves from (1) to another location such as (3), (5), (7), or (9) in one cycle, the system free energy is lowered by the free-energy change arising from the hydrolysis of ATP in aqueous solution, state 1→state 5 in Fig. 3.2. However, the unidirectional movement is not influenced by the changes in the reference value of the solvent free energy because it is governed by the derivative of the potential curve with respect to x multiplied by -1 (i.e., entropic force in x-axis direction).

In the present analysis, the potential in y-axis direction is not considered because in the experiment S1 is artificially confined in the vicinity of F-actin using a special technique [13, 14]. For S1 with geometry 1, the potential in y-axis direction looks like the solid, oscillatory curve in Fig. 2.6. It is extremely difficult for S1 to get detached from F-actin: It is trapped on an RBS. When S1 feels a potential field of the red curve, however, the amplitudes of the potential also become much smaller, and S1 can be released to bulk aqueous solution. In the experiment, such release is prevented by the artificial confinement mentioned above, and the movement of S1 is limited to that in x-axis direction.

According to the physical picture described above, the distance by which S1 moves in x-axis direction on an average per ATP hydrolysis cycle, L_1, is $\sim d_G$. However, the experimental result indicates that it is $\sim 2.5 d_G$ [13, 14]. We then discuss the possible reasons for this discrepancy. In the real system, the switch from the black curve to the red one, for example, does occur not abruptly but rather gradually. Hence, the following additional effect comes into play: As S1 moves along F-actin in the right direction, the potential felt by S1 continues to shift in the lower direction. This shift should promote the movement of S1 by a longer distance and increase L_1. Though this argument is to be investigated in further studies, the physical picture captures such essential points as the crucial importance of the translational displacement of water molecules, roles of the entropic potential field, adjustment of the field depending on geometric properties of S1 by the ATP hydrolysis cycle, and entropic control of the movement of S1 along F-actin. Further, it is consistent with the experimental data [18, 19] showing the following: The binding entropy and enthalpy between S1 and F-actin are both positive and therefore the binding is entropically driven; and the binding entropy for myosin in state 1 or 5 (i.e., with geometry 1) to F-actin is as large as that for myosin in state 4 (i.e., with geometry 1) but much larger than that for myosin in state 2 (i.e., with geometry 2; see Fig. 3.2). The binding entropy is the entropy change which would occur upon S1 binding to F-actin.

3.2.5 Is the Prevailing View Correct?

According to the prevailing view [22, 23], a motor protein functions by converting the free energy of ATP hydrolysis to a work: In the case of the unidirectional movement of S1, for example, the work is necessary for S1 to move against the viscous resistance force by water [22]. We disagree with this view. If it was valid,

the distance by which S1 could move would be the same for all of the hydrolysis cycles. Actually, it sometimes moves by more than a single step and even backward [13, 14]. It should be emphasized that the system comprises not only S1 but also the surrounding aqueous solution: The system does not do a work. Heat is generated but it is absorbed by the external bath. It is interesting that the movement is hindered by water in the prevailing view whereas it is promoted by water in our view.

Of course, with no ATP hydrolysis cycle, the unidirectional movement of S1 is not realized: S1 will not move from an RBS because the system free energy (SFE), which takes the lowest value when S1 is on the RBS, is to be maintained. In the presence of the cycle, the movement of S1 spontaneously occurs, because thanks to the cycle the SFE continues to decrease. After S1 makes a movement per cycle, the SFE becomes lower by the ATP hydrolysis free energy. (This issue is more closely discussed in Sect. 4.2.)

3.3 Insertion and Release of a Solute into and from a Biopolymer Complex: Chaperonin GroEL

Insertion of a solute into a vessel comprising biopolymers followed by release of the same solute from it is a fundamental function in biological systems. We consider two typical examples: (I) An unfolded protein is inserted into chaperonin GroEL from bulk aqueous solution, protein folding occurs within the GroEL cavity, and the folded protein is released back to the bulk solution (a variety of proteins are inserted and released) [2, 24–26]; and (II) an antibiotic molecule is inserted into an ABC transporter from the inside of cell membrane, and then the molecule is released from the transporter to the outside (diverse substrates are carried across the membrane) [27–30]. It is mysterious that the two apparently *opposite* events, insertion and release, successively occur in the same system. By computer simulations, dynamics of structural changes of the transporter itself [31] and characteristics of protein folding within the GroEL cavity [32, 33] have been studied, but neither insertion nor release of a solute has been treated. We note that computer simulations are not capable of covering the time length required to demonstrate insertion or release.

The questions are as follows: How can the solute be inserted into the vessel?; and how can the solute, which has already been inserted and is constrained inside the vessel, be released from it to the outside? Both of insertion and release must be explained consistently using the same theoretical approach. In our opinion, the main physics can be understood through a simplified model: a model focused on solvation properties of a solute in the solvent confined on the scale of a nanometer which are substantially different from those in bulk solvent.

We are concerned with example (I) in this section. GroEL utilizes the ATP hydrolysis cycle: the binding of ATP to GroEL, hydrolysis of ATP into ADP + Pi, and dissociation of Pi and ADP (see Fig. 3.5). First, an unfolded protein is inserted

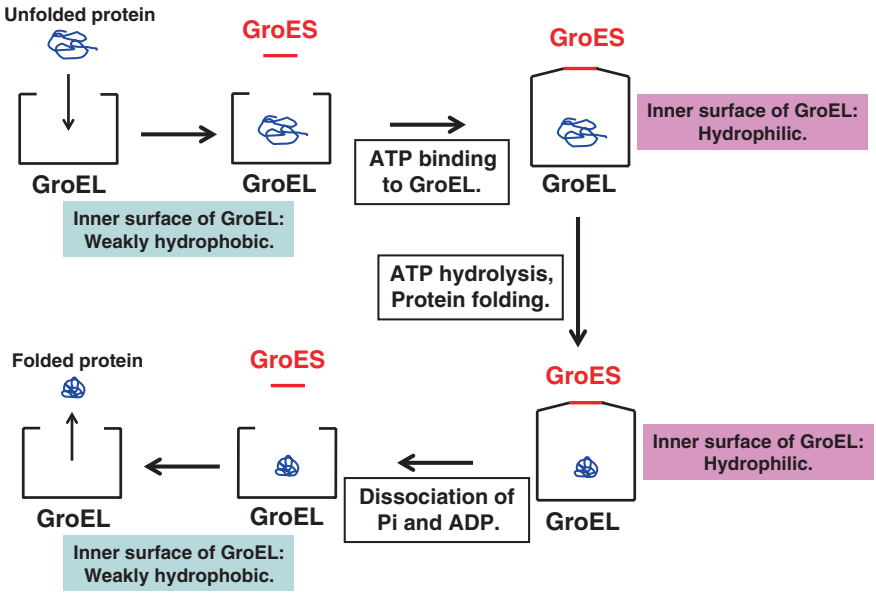

Fig. 3.5 One cycle of ATP hydrolysis (ATP binding, hydrolysis of ATP into ADP+Pi, and dissociation of Pi and ADP) for chaperonin GroEL. Seven APT molecules are hydrolyzed (there are seven binding sites in GroEL). GroEL/GroES (GroES is cochaperonin of GroEL) is considered here but the same illustration is valid for Hsp60/Hsp10 as well (simply replace GroEL and GroES by Hsp60 and Hsp10, respectively)

into GroEL. The ATP binding causes a structural change of GroEL so that the weakly hydrophobic inner surface of GroEL can turn hydrophilic and GroEL can be amenable to the attachment of GroES to its rim. The protein folding occurs within GroEL/GroES. The hydrolysis of ATP also occurs in the course of protein folding. After the folding is finished, Pi and ADP dissociate from GroEL, which is followed by the recovery of the original structure of GroEL. The inner surface of GroEL becomes weakly hydrophobic and GroES is detached from GroEL. The folded protein is then released to the outside. It appears to be very strange that the unfolded protein is inserted whereas the folded one is released.

GroEL works as double-ring complexes in which the two rings act alternately to introduce, encapsulate, and fold a variety of unfolded or denatured proteins [2, 24–26]. However, protein folding occurs even within a single ring and the double-ring system is necessitated only for the dissociation of ADP and Pi followed by detachment of its cochaperonin, GroES [26]. (The dissociation and detachment are driven by a signal transmitted via the binding of ATP to the adjacent ring.) Unlike GroEL/GroES, Hsp60/Hsp10 fully exhibits its function without the formation of double rings [34]. We are concerned not with the difference between GroEL/GroES and Hsp60/Hsp10 but with the mechanism of protein-folding facilitation common in these two complexes.

3.3.1 Model and Theory

The switch from insertion to release for a solute could be achieved by modifying geometric features and inner surface properties of the vessel and/or by altering the conformation of the solute. We believe that the latter is essential in example (I) defined above. Solvation properties of the solute are changed by the alteration of its conformation. A protein, the solute in example (I), becomes much more compact upon folding. Further, the exposed surface of an unfolded protein comprises solvophobic groups as well as solvophilic groups, but that of the folded protein is more solvophilic because solvophobic groups are somewhat preferentially buried during the folding process.

We wish to adopt the simplest possible model that still captures the essential physics [2]. A large sphere with diameter d_B (solute 1) and a cylindrical vessel (solute 2), which are illustrated in Fig. 3.6, are immersed in the solvent at infinite dilution. Figure 3.6 also shows the coordinate system chosen. The solvent is modeled as small hard spheres with diameter d_S interacting through the hard-sphere potential with the attractive part of the Lennard-Jones potential expressed as $u_{SS}(r) = -\varepsilon(d_S/r)^6$ for $r > d_S$ ($\varepsilon/(k_BT) = 1.0$ for $T = 298$ K) where r is the distance between the centers of two small spheres. The bulk-solvent density ρ_S and d_S are set at those of water under the normal condition: $\rho_S {d_S}^3 = 0.7317$ ($d_S = 0.28$ nm). The solute I-solvent ($I = 1, 2$) interaction potential is taken to be $u_{IS}(h) = \infty$ for $h < d_S/2$, where h is the distance between the center of a small sphere and the nearest surface of solute I. In $u_{IS}(h)$ for $h > d_S/2$, which includes an important parameter ξ_I (>0), the repulsive part of the 9–3 type potential is simply replaced by a hard-core interaction and the potential at large separations is truncated [2]. As ξ_I increases, the attractive part of $u_{IS}(h)$ becomes stronger. To focus on the effects of properties of solute 1, geometric features of solute 2 and ξ_2 are all fixed ($\xi_2/(k_BT) = 1.5$ for $T = 298$ K), and ξ_1 and d_B are varied as major parameters. When ξ_1 is small

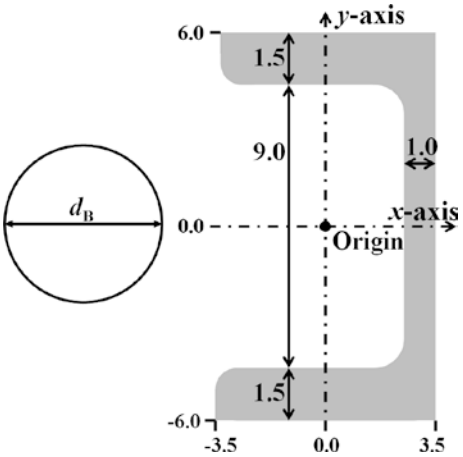

Fig. 3.6 Large sphere and cross section of vessel considered ($z = 0$). The numbers given are scaled by d_S. When the large sphere diameter d_B is set at $5d_S$, for example, the center of the large sphere in contact with the bottom wall is at $(x, y) = (0, 0)$

relative to ε, solute 1 is solvophobic, and when ξ_1 is large relative to ε, solute 1 is solvophilic. The functional forms of $u_{SS}(r)$ and $u_{IS}(h)$ are unimportant.

We analyze the PMF between solutes 1 and 2 immersed in the solvent using the 3D-IET [15–17]. Here, we describe how to specify the solute I-solvent ($I = 1, 2$) potential for solute 2 ($I = 2$). In the 3D-IET, the numerical values of the potential are calculated on 3D grid points. On each grid point, we determine the distance between the center of the small sphere placed on this grid point and the nearest surface of the vessel. The distance is then substituted into h for calculating the potential. With this treatment, the cylindrical dependence of the potential can fully be taken into account: A small sphere feels significant, negative potential only near the base surface as well as the side one of the vessel, and the potential becomes progressively weaker as the small sphere is more separated from the surface. This property is all we need for the spatial distribution of the solute 2-solvent potential. Further, we have verified for solutes 1 and 2 that the results obtained are quite robust against how to truncate the potential at large separations.

Since soft (attractive) interaction potentials are incorporated in the model, the PMF possesses the energetic and entropic components ($-T\Phi_S$ and Φ_E, respectively). They are obtained from "$\Phi_S = -(\partial\Phi/\partial T)_V = -\{\Phi(T + \delta T) - \Phi(T - \delta T)\}/(2\delta T)$ ($\delta T = 5$ K) and $\Phi_E = \Phi + T\Phi_S$". We are particularly interested in Φ, $-T\Phi_S$, and Φ_E scaled by k_BT within the vessel cavity, which are largely influenced by the solvent structure within it. The entropic component is referred to as "entropic potential."

3.3.2 Entropic Insertion of a Solute into a Vessel

The spatial distribution of $\Phi/(k_BT)$ on the cross section $z = 0$ and its components, $\Phi_E/(k_BT)$ and $-\Phi_S/k_B$, are shown in Fig. 3.7 [2]. In Fig. 3.7a, a domain within which the solute is highly stabilized appears around the x-axis. It is difficult for the solute to overcome a free-energy barrier scaled by k_BT well exceeding 1. As explained in the figure caption, the solute is most likely to be inserted into the vessel through the route indicated by the white dotted arrow and constrained within the small space around the position indicated by "−5.9" (i.e., almost in the center of the vessel cavity). This behavior is in accord with the experimental observation that a protein inserted into GroEL is confined within the cavity without contacting the GroEL surface. The distribution and its components are symmetrical with respect to the x-axis. The route given by the white dotted arrow is just an example one, and the route that is symmetrical with respect to the x-axis is also equally probable. We then compare Φ, Φ_E, and $-T\Phi_S$ within the domain around the x-axis. Insertion and constraint of the solute is achieved primarily not by the energetic component in Fig. 3.7b but by the entropic one in Fig. 3.7c. We have shown that even with $\varepsilon = \xi_1 = \xi_2 = 0$ the solute is inserted into the vessel and strongly confined within a small space almost in the center of the vessel cavity [2].

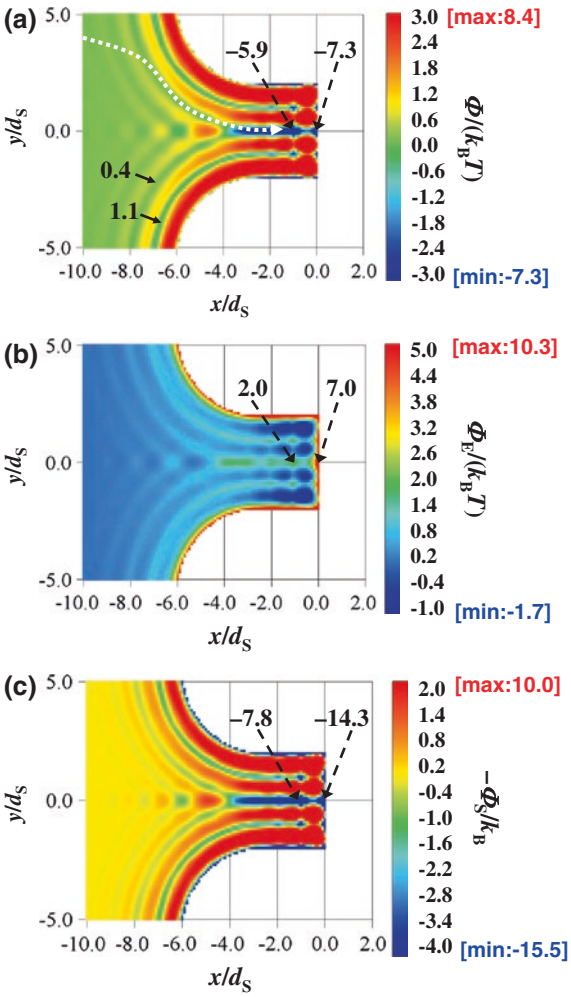

Fig. 3.7 Spatial distribution of $\Phi/(k_BT)$ (Φ is the potential of mean force) (**a**), $\Phi_E/(k_BT)$ (**b**), and $-\Phi_S/k_B$ (**c**) on the cross section $z = 0$ between the large sphere and the vessel immersed in small spheres. As the color approaches *thick blue*, they become lower, and as the color approaches *thick red*, they become higher ("max" and "min" represent the maximum and minimum values, respectively). $\Phi = \Phi_E - T\Phi_S$, $\xi_1/(k_BT) = 1.5$ for $T = 298$ K, and $d_B = 5d_S$. T, k_B, d_B, and d_S denote the absolute temperature, Boltzmann constant, diameter of the large sphere, and diameter of the small spheres, respectively. The positions where $\Phi_E/(k_BT)$ takes the maximum and minimum values are different from those where $-\Phi_S/k_B$ takes the maximum and minimum values, respectively. The center of the large sphere cannot enter the domain drawn in white. The value at the position indicated by a black broken arrow is also given. Between the start and end points of a black solid arrow, there is a free-energy barrier indicated by the number. In (**a**), the large sphere must overcome a barrier scaled by k_BT of ~4 to move from the position of "−5.9" to that of "−7.3": It is constrained within the small space around the position indicated by "−5.9"

In Fig. 3.7c, $-\Phi_S/k_B$ takes large, negative values when the distance between the nearest solute and vessel surfaces is ~nd_S (n is 0, 1, and 2) and that between the farthest surfaces is $(4 - n)d_S$. This is because the small spheres (i.e., solvent particles) can efficiently be packed within the domain confined between the solute and vessel surfaces. This efficient packing is advantageous from the viewpoint of solvent entropy [2]. When the nearest distance is not ~nd_S, the vacant space which is unavailable to the small spheres unavoidably appears within the domain. This generation of the vacant space is entropically unfavorable [2].

3.3.3 Release of a Solute from a Vessel: Switch from Insertion to Release

On the basis of parametric studies, we obtain the following information on Φ_E [2]. In the case where the inner surface of the vessel is more or less solvophobic, Φ_E acts for insertion when the solute is solvophobic and for release when it is solvophilic. The solvent density within the cavity of a solvophobic vessel is, on the whole, lower than in the bulk. Hence, a solvophilic solute is preferentially solvated in bulk solvent, whereas a solvophobic solute tends to be excluded from the bulk and inserted into the vessel cavity. In what follows, we describe two important findings [2]. First, a decrease in the solute size d_B gives only smaller EV for solvent molecules, leading to weaker entropic force and smaller amplitudes of $-T\Phi_S$ (i.e., smaller $|-T\Phi_S|$). As a consequence, the insertion power induced by $-T\Phi_S$ becomes weaker as d_B decreases. Second, Φ_E is strongly dependent on the solute-solvent and vessel inner surface-solvent affinities, whereas $-T\Phi_S$ is rather insensitive to them (this insensitivity plays significant roles in Sect. 3.4.3).

The solute size needs to be made smaller for releasing the solute, which has already been inserted into the vessel and is constrained inside it, to the outside. The EV then decreases, leading to a reduced insertion power induced by $-\Phi_S$. At the same time, when the solute solvophilicity is sufficiently increased and the vessel inner surface is rather solvophobic, Φ_E acts for release. If Φ_E is dominant, the solute is released. This argument is demonstrated in Fig. 3.8 [2]. As observed in Fig. 3.8a, the solute is most likely to be released from the vessel cavity to the outside through the route indicated by the white dotted arrow. The release is made possible not by the entropic component of the PMF shown in Fig. 3.8c but by the energetic one shown in Fig. 3.8b. Since the unfolded protein generates large EV, it feels $-\Phi_S$ which strongly drives its insertion into GroEL. Its overall solvophilicity is low, and Φ_E felt by it promotes only weak release or insertion: It is inserted. The folded protein, by contrast, possesses smaller EV and much higher overall solvophilicity, and $-\Phi_S$ drives its insertion less strongly while Φ_E powerfully acts for release: It is released. A protein molecule is heterogeneous in the sense that hydrophobic and hydrophilic groups are almost randomly distributed within it. Even after its folding is completed, the increase in its surface hydrophilicity is not very large. Therefore, the reduction in its EV is also required for the release.

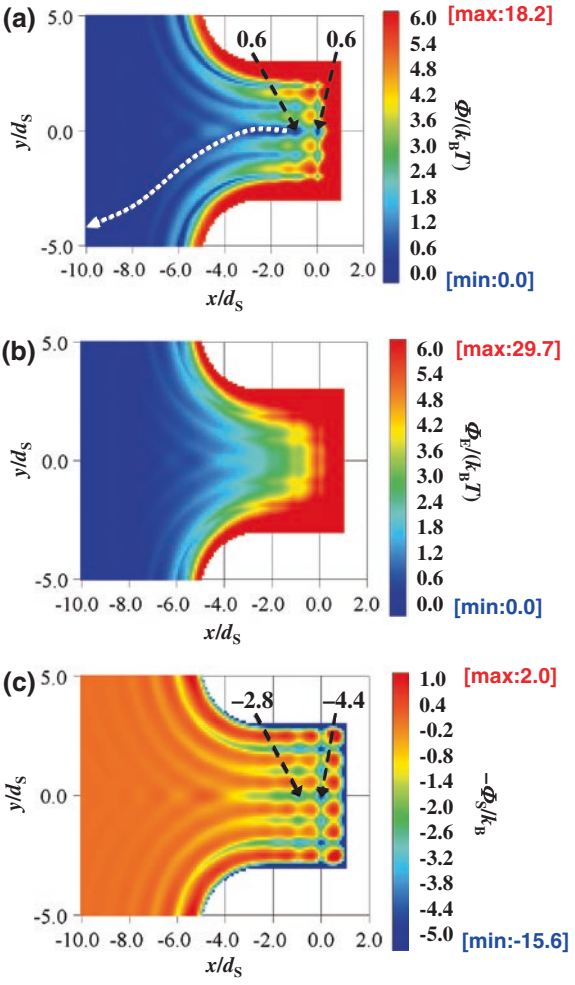

Fig. 3.8 Spatial distribution of $\Phi/(k_BT)$ (Φ is the potential of mean force) (**a**), $\Phi_E/(k_BT)$ (**b**), and $-\Phi_S/k_B$ (**c**) on the cross section $z = 0$ between the large sphere and the vessel immersed in small spheres. As the color approaches *thick blue*, they become lower, and as the color approaches *thick red*, they become higher ("max" and "min" represent the maximum and minimum values, respectively). $\Phi = \Phi_E - T\Phi_S$, $\xi_1/(k_BT) = 3.0$ for $T = 298$ K, and $d_B = 3d_S$. T, k_B, d_B, and d_S denote the absolute temperature, Boltzmann constant, diameter of the large sphere, and diameter of the small spheres, respectively. The center of the large sphere cannot enter the domain drawn in *white*. The value at the position indicated by a *black broken arrow* is also given

The entropic component of the PMF usually drives the insertion process while the energetic component can be requisite in the release process. The insertion/release function is exhibited through judicious adjustment of these two components.

3.3.4 Roles of GroES as a Lid

GroES works as a lid (see Fig. 3.5). We have performed additional calculations using a simple lid model and the vessel [2]. The findings are as follows: With the lid attachment, the PMF-values near the lid surface undergo significantly large

changes; both the unfolded protein and the folded one, which cannot contact the lid surface, remain constrained within a small space almost in the center of the GroEL cavity; and the constraint becomes stronger as the solvophilicity of the inner surface of GroEL increases, because the PMF near the inner surface takes progressively large, positive values with the increase in its solvophilicity. It is known that by the structural change of GroEL caused by the ATP binding mentioned above, the inner surface of GroEL becomes more hydrophilic. Thus, the ATP binding leads to stronger constraint of the protein.

The hydrolysis of ATP occurs in the course of protein folding. After the folding is finished, the dissociation of Pi and ADP occurs. This is followed by the recovery of the original structure of GroEL and detachment of the lid, leading to the PMF looking like that in Fig. 3.8. The folded protein is then released to the outside. (Another finding from our theoretical study is that the inner surface of GroEL should not be hydrophilic for the release to occur: The inner surface turns more hydrophobic upon dissociation of Pi and ADP.) It is apparent that GroES acting as a lid is useful for safely preventing the energetic release before the folding is finished.

3.3.5 Mechanism Through Which a Chaperonin Works

In summary, a chaperonin exhibits its high function by making the most of the following three factors [2]: (i) anomalous hydration properties of a protein in the water confined on the scale of a nanometer, (ii) changes in conformation and properties of the protein upon folding, and (iii) structural changes of the chaperonin adjusted by the ATP binding, hydrolysis, and dissociation of Pi and ADP. The basic physics is rather simple, and specific, chemical characteristics of a protein are not important. The characteristics, "the folded state is more hydrophilic and compact than the unfolded state," are shared by a variety of proteins: They are inserted and released for both GroEL and Hsp60, which is in accord with the experimental evidence.

3.3.6 Dynamics of Insertion/Release Process

The subject which remains unresolved is the dynamics: the solute movement in the presence of an entropic potential field. We have recently developed a theoretical method formulated using the Fokker–Planck equation and illustrated it for the entropic insertion of a spherical solute into a cylindrical vessel [35]. The spatial distribution of vessel-solute entropic potential is used as part of the input data. The key quantity analyzed is the density of the probability of finding the solute at any position at any time. The following have been verified: The solute is inserted along the central axis of the vessel cavity and trapped at a position where the entropic potential takes a local minimum value; the solute keeps being trapped without touching the vessel inner surface; in a significantly long time τ, the solute transfers

to the position in contact with the vessel bottom possessing the global potential minimum along the central axis; and as the solute size increases, τ becomes remarkably longer. It has been shown for a small protein with ~100 residues that τ is long enough for it to complete the folding.

3.4 Transport of Diverse Substrates Across Membrane by an ABC Transporter

For an ABC transporter [5, 36] in example (II) defined in Sect. 3.3, the properties of a substrate remain almost unchanged during the insertion/release process unlike those of a protein. Hence, the switch from insertion to release should be achieved by modifying geometric features or inner surface properties of the transporter. The transporter takes the inward-facing structure for insertion while it takes the outward-facing structure for release as illustrated in Fig. 3.9. The binding of ATP to the transporter causes the change from the inward-facing structure to the outward-facing one. Hydrolysis of ATP followed by dissociation of Pi and ADP leads to the change from the outward-facing structure to the inward-facing one. Since the two structures are quite different, the corresponding spatial distributions of the transporter-substrate PMF are also substantially different.

A notable feature of the ABC transporter is the multidrug efflux [27] implying that it can handle a variety of substrates (i.e., drugs). If the insertion and release events in the transporter were controlled by the energetic component of the PMF as in a chaperonin, it would be impossible to handle both of solvophobic and solvophilic solutes because the affinities and sizes of drugs are invariant during the

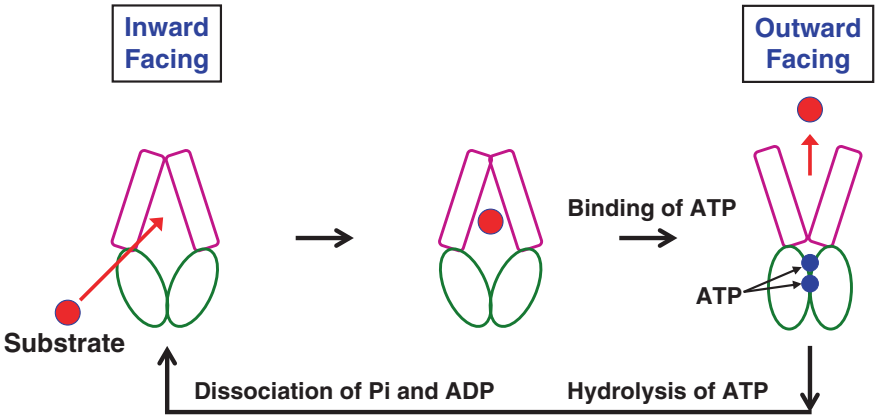

Fig. 3.9 One cycle of ATP hydrolysis for an ATP-binding cassette (ABC) transporter: Insertion and release of a substrate. Two ATP molecules are hydrolyzed (there are two binding sites in the transporter)

insertion/release process. When the inner surface of the transporter is solvophobic, only a solvophilic drug is released: When it is solvophilic, only a solvophobic drug is released. Therefore, the switch from insertion to release in the multidrug efflux transporter must be achieved by the entropic component when it dominates, since the entropic component is rather insensitive to the solute-solvent affinity, solvophobic or solvophilic. The entropic component dominates when the inner surface of the transporter is neither solvophobic nor solvophilic. With such an inner surface, the space within the transporter and the bulk are equally favorable both for solvophobic and solvophilic drugs from the viewpoint of energetic component. The drug must be released entropically.

It has been shown in Sects. 3.3.2 and 3.3.3 that the entropic component of the PMF always acts for insertion. However, this conclusion is valid only when the vessel geometry is fixed. The structural change caused by the ATP binding can play essential roles in the switch from insertion to release. In this section, we present some informative calculation results [27]. We show that once the solute is inserted, it can be released *entropically* by changing the spatial distribution of the entropic potential *using continuous variation of the vessel geometry*. Both insertion and release can be achieved by the entropic component of the PMF. Moreover, solutes with a wide range of sizes can be released using the same manner of vessel-geometry variation.

3.4.1 Model and Theory

We consider rigid-body models in which the constituents interact only through hard-body potentials: a big hard vessel and a big hard sphere immersed at infinite dilution in small hard spheres with diameter d_S forming the solvent. The big sphere corresponds to a solute and its diameter is d_B. The initial geometry of the vessel is shown in Fig. 3.10a: It is cylindrical and the right side (i.e., "exit" for the solute) is closed. It corresponds to the inward-facing structure shown in Fig. 3.9. The Cartesian coordinate system is chosen as illustrated in the figure. After the solute insertion, the vessel geometry is varied as explained in Fig. 3.10b–d: The exit is opened and the diameter of a portion in the entrance side is made smaller by $2d_S$, and this portion is continuously lengthened. This geometric variation mimics the transition to the outward-facing structure shown in Fig. 3.9. The cross section of $z = 0$ is shown for each geometry. Due to the rigid body models, the vessel-solute PMF possesses only the entropic component.

3.4.2 Entropic Release of a Solute from a Vessel

In the ABC transporter, the solute insertion occurs spontaneously as discussed in Sect. 3.3.2. In TolC of the drug efflux pump, AcrA/AcrB/TolC (see Sect. 3.6), it is made with the aid of AcrB: AcrB interacting with TolC sends the solute to the

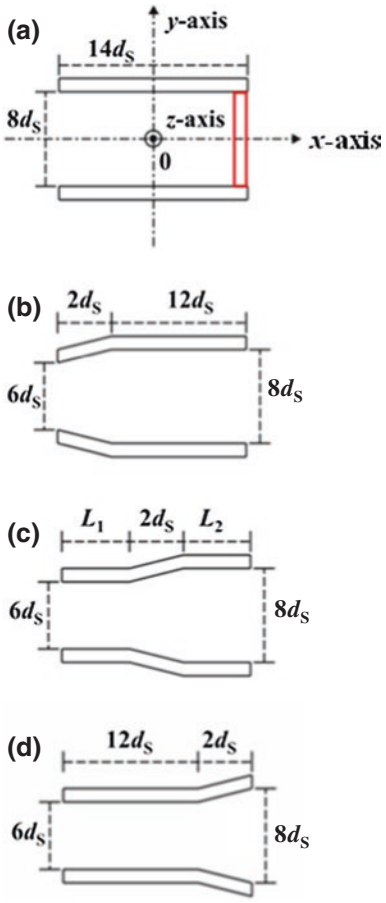

Fig. 3.10 Variation of vessel geometry: (**a**)→(**b**)→(**c**)→(**d**). The geometry in (**a**) is a cylinder with inner diameter $8d_S$, length $14d_S$, and thickness d_S (d_S is the molecular diameter of the solvent). The coordinate system is chosen as illustrated here. The cross section of $z = 0$ is shown for each geometry. Though the geometry variation is illustrated in a stepwise manner, it is made *continuously*

central position within the vessel cavity of TolC. Right after the solute is inserted, the vessel geometry is continuously varied as illustrated in Fig. 3.10b–d. This vessel-geometry variation leads to the change in the spatial distribution of the entropic potential: See Fig. 3.11.

A notable point is that the entropic potential is time dependent [27]. There are three different time scales: those of the solvent motion, variation in the vessel geometry, and solute motion. The time scale of the solvent motion is doubtlessly the fastest. The solvent is practically in equilibrium with the vessel-solute configuration all the time. The variation of vessel geometry is followed by that of entropic potential with no time lag. We assume that these variations are relatively faster than the solute motion. In the real system, the faster variation of vessel geometry could be realized by the ATP binding to the ABC transporter. It follows that an entropic force, which is given as $F_S = -\{\partial(-T\Phi_S)/\partial x\}$, *continuously* acts on the solute in the right direction along the x-axis (i.e., in the axial direction toward the exit) and continues to accelerate its motion during the vessel-geometry variation

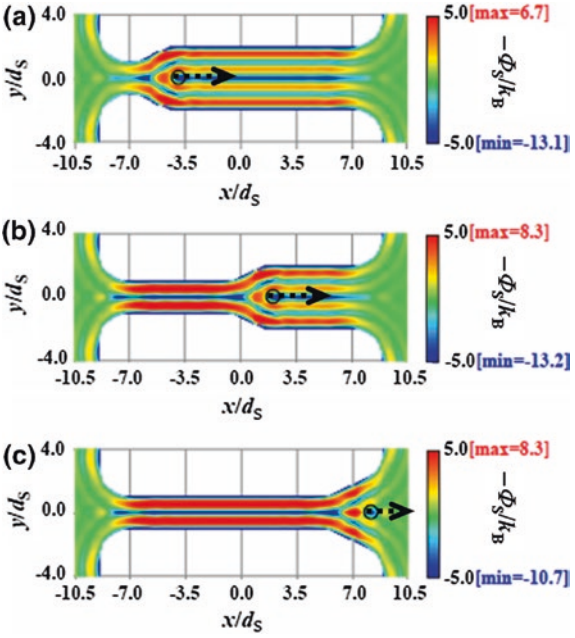

Fig. 3.11 Distributions of $-\Phi_S/k_B$ (Φ_S and k_B are the vessel-solute entropic potential and the Boltzmann constant, respectively) on the cross section of $z = 0$ for vessel geometries (b), (c), and (d) illustrated in Fig. 3.10b, c and d, respectively. The solute size d_B is $4d_S$ (d_S is the solvent diameter). $-\Phi_S/k_B$ becomes lower as the color approaches *dark blue*, and it becomes higher as the color approaches *dark red* ("max" and "min" represent the maximum and minimum values, respectively). The *open circle* indicates the position where the entropic potential is locally minimum

(see Fig. 3.11). When vessel geometry (d) is reached, the solute should possess a considerably high velocity in x-axis direction. As a consequence, even when a barrier well exceeding k_BT is present, the solute can readily overcome it. A larger solute is subjected to a stronger force, and the solute velocity at the exit becomes higher as the solute size or the vessel length increases. It is quite interesting and important that such rich behavior is observed in the very simple model system adopted by us.

After the solute release, Pi and ADP dissociate, the transporter structure returns to the other one, and the next solute insertion occurs. We have also shown that when the entropic component of the vessel-solute potential of mean force dominates, solutes with a variety of sizes can be inserted and released using the same manner of vessel-geometry variation [27]: That is, the multidrug efflux can be achieved. The multidrug efflux is in marked contrast with the high selectivity pertaining to the receptor-ligand binding. Nevertheless, both of them are guided by the solvent-entropy effect.

3.4.3 Multidrug Efflux

The energetic component of the PMF is strongly dependent on the solute-solvent and vessel inner surface-solvent affinities, whereas the entropic component is rather insensitive to them. The basis of our physical picture is that the multidrug

efflux can be assured under a condition where the inner surface of the vessel is neither solvophobic nor solvophilic and the entropic component dominates. As long as the vessel geometry is fixed, however, the entropic component does not work for release. A solute which has been inserted can also be released entropically using a continuous variation of the vessel geometry [27]. The variation is achieved by the ATP binding in an ABC transporter. In TolC, the proton motive force causes structural changes of AcrB, and these changes are transmitted to TolC through AcrA, possibly leading to a continuous vessel-geometry variation of TolC (see Sect. 3.6). Moreover, an MD simulation study [37] has suggested that TolC can vary its geometric characteristics even by itself (an observed variation is a peristaltic motion of the periplasmic domain). Thus, the continuous variation of the vessel geometry is never unrealistic.

Once a solute is inserted into the ABC transporter or sent from AcrB to the central position within the TolC cavity, the solute must be ejected to the external medium through the exit before the next solute is inserted or sent: The ejection of every solute needs to be finished with sufficient rapidness. This requirement can certainly be met when the solute motion is directed only toward the exit. This unidirectional motion is assured by the time-dependent entropic force. Our physical picture of the multidrug efflux is clearly distinguished from the general view assuming the existence of multifunctional ligand-binding sites [38–40] to which various types of solutes can bind and relying on the mere diffusion (i.e., diffusion in the presence of no particular potential field) of a solute for the insertion/release process. In this view, once a solute binds to such a site, it may be difficult to make the solute dissociate from the site. Further, the requirement mentioned above cannot be met.

3.5 Rotation of Central Subunit Within F_1-ATPase

F_1-ATPase [3, 4], a water-soluble part in the F_oF_1-ATP synthase, is a rotary motor which has been studied rather extensively in experiments. The central stalk (i.e., γ subunit) of the $\alpha_3\beta_3\gamma$ complex taken from F_1-ATPase has been shown to exhibit a directed rotation. The $\alpha_3\beta_3\gamma$ complex is the most fundamental unit best suited to the investigation of the rotational mechanism of a rotary motor. In this complex, the $\alpha_3\beta_3$ subunits are arranged hexagonally around the γ subunit [41] as shown in Fig. 3.12. By utilizing the ATP hydrolysis cycle, the γ subunit rotates in a counterclockwise direction when viewed from the F_o side. We discuss the rotation mechanism with the emphasis on the water-entropy effect.

One of the most probable structures of the $\alpha_3\beta_3\gamma$ complex, which has experimentally been determined [41], is illustrated in Fig. 3.12 (also see Fig. 3.13a). ATP is bound to the β subunit named β_{TP}. ATP is also bound to the β subunit named β_{DP}, but ATP within β_{DP} is ready to be hydrolyzed into ADP+Pi. None of ATP and ADP is bound to the β subunit named β_E (Pi remains within β_E). The three α subunits are named α_{TP}, α_{DP}, and α_E, respectively, as shown in the figure.

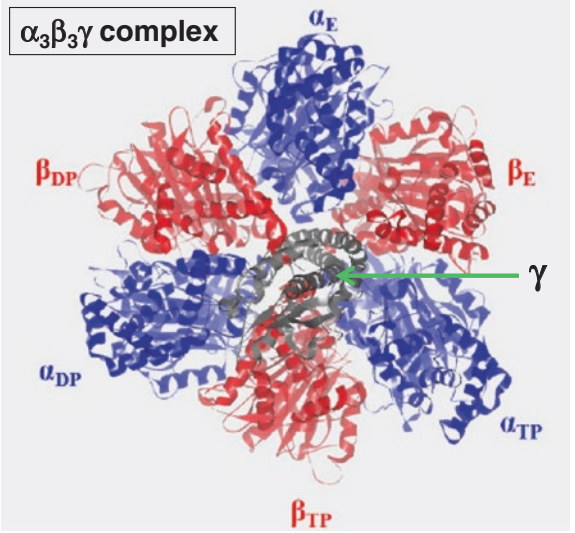

Fig. 3.12 Ribbon representation of the $\alpha_3\beta_3\gamma$ complex viewed from the F_o side. This figure is drawn using the DS visualizer 2.5

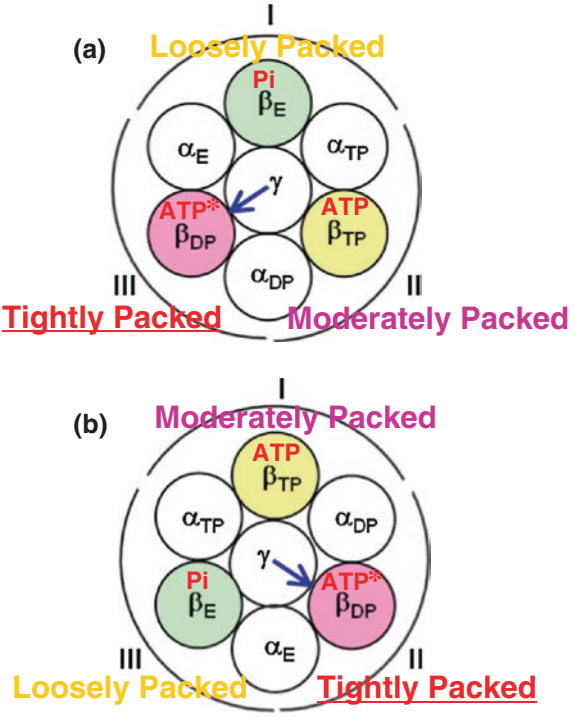

Fig. 3.13 One cycle of ATP hydrolysis for F_1-ATPase: 120° rotation of the γ subunit. One ATP molecule is hydrolyzed. ATP* denotes ATP that is ready to be hydrolyzed into ADP + Pi. **a** Overall conformation of the $\alpha_3\beta_3\gamma$ complex shown in Fig. 3.12. **b** Overall conformation after the 120° rotation of the γ subunit

The conformations of the three β subunits are significantly different from one another [42–44]. We define the following three sub-complexes as illustrated in Fig. 3.13a, "Sub-complex I: γ, β_E, α_E, and α_{TP}", "Sub-complex II: γ, β_{TP}, α_{TP}, and α_{DP}", and "Sub-complex III: γ, β_{DP}, α_{DP}, and α_E" [3, 4]. The γ subunit performs a 120° step rotation during one ATP hydrolysis cycle [45]. As observed in Fig. 3.13, the overall conformations of the $\alpha_3\beta_3\gamma$ complex before and after the 120° rotation are the same. The sub-complexes are named I, II, and III in terms of their positions in the structure. For example, when the γ subunit rotates by 120°, the arrangement changes as shown in Fig. 3.13b and sub-complex III, for example, now comprises γ, β_E, α_E, and α_{TP}.

3.5.1 Summary of Experimental Observations

We start with Fig. 3.14a. Both of β_{TP} and β_{DP} are in closed conformations while β_E adopts an open conformation. Though the details of the rotational behavior experimentally observed are rather controversial, we adopt the following [3, 4, 42–46] (we note, however, that our physical picture is independent of the details):

(1) Pi dissociates from β_E and the hydrolysis of ATP occurs within β_{DP}, with the result that β_{DP} changes its conformation into a half-open one [44]. The β subunit with the half-open conformation is denoted by β_{DP}^{HO}. This conformational change of β_{DP} leads to the 40° rotation of the γ subunit [46]. The $\alpha_3\beta_3\gamma$ complex now takes the overall conformation shown in Fig. 3.14b. Primes are added to the subunits in Fig. 3.14b because their conformations should be different from those in Fig. 3.14a. The details of the overall conformation in Fig. 3.14b are not known, but it is unambiguous that β'_E, β_{DP}^{HO}, and β'_{TP} are in open, half-open, and closed conformations, respectively [44].

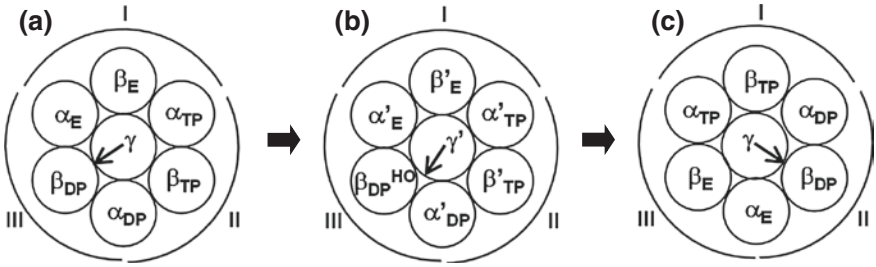

Fig. 3.14 **a** Overall conformation of the $\alpha_3\beta_3\gamma$ complex shown in Fig. 3.12. (Fig. 3.14a is the same as Fig. 3.13a.) **b** Overall conformation after the 40° rotation of the γ subunit. **c** Overall conformation after the 80° rotation of the γ subunit. The arrow of the γ subunit points toward the most tightly packed region. The conformational change (a)→(b) is caused by the dissociation of Pi from β_E and hydrolysis of ATP within β_{DP}. The conformational change (b)→(c) follows the ATP binding to β'_E and dissociation of ADP from β_{DP}^{HO}

(2) ADP dissociates from β_{DP}^{HO} and ATP binds to β'_E. The conformational changes "$\beta'_E \rightarrow \beta_{TP}$ and $\beta_{DP}^{HO} \rightarrow \beta_E$" occur, accompanying the 80° rotation of the γ subunit [44]. The $\alpha_3\beta_3\gamma$ complex now takes the overall conformation shown in Fig. 3.14c that is the same as Fig. 3.13b. We note that Fig. 3.14a, c share the same overall conformation.

3.5.2 Model and Theory

Ito and Ikeguchi [47] have found that the packing efficiency of the $\alpha_3\beta_3\gamma$ complex is nonuniform. We pay attention to this nonuniformity and analyze it more closely [3, 4]. The hydration entropy (HE) is the key quantity in analyses on the packing efficiency of the $\alpha_3\beta_3\gamma$ complex. We calculate the HEs not only of the three sub-complexes but also of α, β, and γ subunits and of α-β, α-γ, and β-γ subunit pairs. ΔS_{ij} is defined as "$\Delta S_{ij} = S_{ij} - S_i - S_j$" where S_{ij} is the HE of subunit pair $i-j$ and S_i is the HE of subunit i ($i = \alpha_E$, α_{TP}, α_{DP}, β_E, β_{TP}, and β_{DP}). Subunit j is the subunit adjacent to subunit i. ΔS_{ij} represents the water-entropy gain upon formation of subunit pair $i-j$. Smaller $|S_i|$ ($S_i < 0$) implies that the backbone and side chains of subunit i are more efficiently (closely) packed. ΔS_{ij} ($\Delta S_{ij} > 0$) becomes larger as the efficiency (tightness) of interface packing between subunit pair $i-j$ increases. The HE is calculated using the ADIET-MA hybrid explained in Sect. 2.6. The crystal structure of bovine heart mitochondria [47, 48] (PDB CODE: 2JDI) is employed in the analyses.

3.5.3 Nonuniform Packing Efficiency in F_1-ATPase

The results of the HE analyses [3, 4] indicate that the packing efficiency in the $\alpha_3\beta_3\gamma$ complex is highly nonuniform. The γ subunit with a special orientation, β_{DP}, α_{DP}, and α_E are most tightly packed. In Figs. 3.13a or 3.14a, the absolute value of the HE of sub-complex III is the smallest among the three sub-complexes: It is smaller than that of sub-complex II by ~$410k_B$ and that of sub-complex I by ~$630k_B$. Since the conformations of the complex before and after the 120° rotation of the γ subunit are the same, there is no water-entropy change upon the 120° rotation. However, the free energy of the system reduces by the free-energy change upon the ATP hydrolysis in aqueous solution, F_H (F_H is roughly -50 kJ/mol: ~$-20k_BT$ ($T = 298$ K)). It is interesting to note that the rotation leads to a water-entropy loss of ~$-630k_B$ in sub-complex III and to water-entropy gains of ~$220k_B$ and ~$410k_B$ in sub-complexes I and II, respectively. Strikingly, their absolute values are much larger than $|F_H/T|$. Any loss caused in one of the sub-complexes during the rotation is somewhat compensated with the gains occurring in the other sub-complexes. Without this compensation, the $\alpha_3\beta_3\gamma$ complex would undergo a significantly large free-energy barrier hindering a smooth rotation.

As explained in Sect. 2.8, from the viewpoint of the entropic EV effect, it is desired for a protein (or a complex of proteins) that all of the backbone and side chains be tightly packed. However, this is not always possible (an arbitrary amino acid sequence is usually incapable of achieving such overall tight packing; even the sequences present in biological systems are often incapable). Even in the case where the overall tight packing is not achievable, there are certainly the portions that can tightly be packed. It is important to pack such portions *preferentially*. For example, the native structure of yeast frataxin [49] has a large valley and a tail, as shown in Fig. 3.15. Nevertheless, $|S|$ (S is the hydration entropy: the loss of water entropy upon solute insertion) of the native structure is almost minimized because the other portions are tightly packed. If a uniform packing was undertaken, the valley and/or the tail could be removed, but the resultant overall packing would become rather loose, causing a larger value of $|S|$. A similar feature is found for the $\alpha_3\beta_3\gamma$ complex. In the situation that two of the β subunits (β_{DP} and β_{TP}) are in closed conformations and the other (β_E) takes an open conformation, the water entropy in the presence of the $\alpha_3\beta_3\gamma$ complex immersed is maximized when the tight packing in β_{DP}, α_{DP}, α_E, and the γ subunit with a special orientation is locally formed. The packing in the other portions is less important. The uniformity would result in looser overall packing and lower water entropy. Interestingly, its nonuniform packing efficiency plays pivotal roles in the rotation mechanism [3, 4].

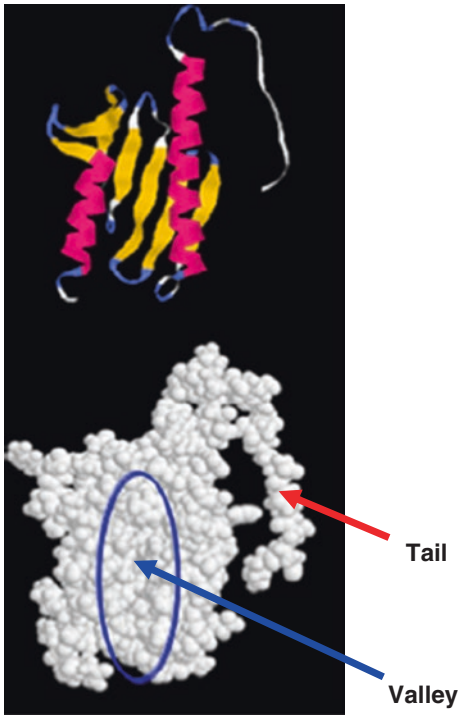

Fig. 3.15 Illustration of the native structure of yeast frataxin (PDB CODE: 2ga5) drawn by the DS visualizer 2.5. It has a large valley and a tail

3.5.4 Physical Picture of Rotational Mechanism

We define the orientation of the γ subunit as follows. As shown in Fig. 3.12, the γ subunit has a warped shape with a slightly concave portion and a protruding portion when it is viewed from the F_o side. Tightly packed interfaces are formed between the residues Arg8-Ile19 in the γ subunit and the residues Asp386-Leu391 in β_{DP} [47]. The residues Arg8-Ile19 are in the slightly concave portion of the γ subunit, indicating that the tight packing is formed between this portion and β_{DP}. This portion is referred to as portion X. The vector inking centers of the $\alpha_3\beta_3\gamma$ complex and portion X can be used as a guide of the orientation of the γ subunit (see Fig. 3.14). It is important to note that the interface between the γ subunit and β_E interacting with the protruding portion is loosely packed.

The $\alpha_3\beta_3\gamma$ complex is packed with nonuniform efficiency so that the entropy of water in which it is immersed can be made as high as possible. The tightest packing is formed in sub-complex III in Fig. 3.14a. The vector representing the orientation of the γ subunit points toward the most tightly packed region of the $\alpha_3\beta_3\gamma$ complex, sub-complex III. Our physical picture [3, 4] can be summarized as follows:

1. The conformational change of β_{DP} into $\beta_{DP}{}^{HO}$, which follows the dissociation of Pi from β_E and hydrolysis of ATP within β_{DP}, induces a looser packing in sub-complex III comprising β_{DP}, α_{DP}, α_E, and the γ subunit. This conformational change would cause a decrease in water entropy. For preventing the water-entropy decrease, the structure of the $\alpha_3\beta_3\gamma$ complex is reorganized. In Fig. 3.14a, the water entropy was almost maximized by giving preference to the packing in sub-complex III. However, sub-complex III is no more amenable to such preferential packing, and priority is transferred to the packing in sub-complexes II and I: The better choice is the former which is already more tightly packed than the latter. As a consequence, the packing in sub-complex II becomes tighter while that in sub-complex III becomes looser, which is completed together with the rotation of the γ subunit toward the more tightly packed region (i.e., by 40° in a counterclockwise direction; the angle 40° comes from the experimental observation). With this reorganization of the packing structure of the $\alpha_3\beta_3\gamma$ complex, the water-entropy decrease described above, which would be caused, is judiciously suppressed.
2. ADP dissociates from $\beta_{DP}{}^{HO}$ and ATP binds to β'_E. It is probable that the conformation of a β subunit becomes closed upon ATP or ADP binding and open upon ATP or ADP dissociation. The ADP dissociation causes the conformational change, $\beta_{DP}{}^{HO} \rightarrow \beta_E$. This conformational change would cause a decrease in water entropy. For preventing the water-entropy decrease, the structure of the $\alpha_3\beta_3\gamma$ complex is reorganized. By the ATP binding, the conformational change, $\beta'_E \rightarrow \beta_{TP}$, occurs. Namely, $\beta_{DP}{}^{HO}$ and β'_E change their conformations to open and closed conformations, respectively, toward the recovery of the overall conformation shown in Fig. 3.14a. After β'_{TP} becomes closed ($\beta'_{TP} \rightarrow \beta_{DP}$), the γ subunit rotates by 80° in a counterclockwise direction: The tight packing in sub-complex III in Fig. 3.14a is thus recovered in sub-complex II in Fig. 3.14c.

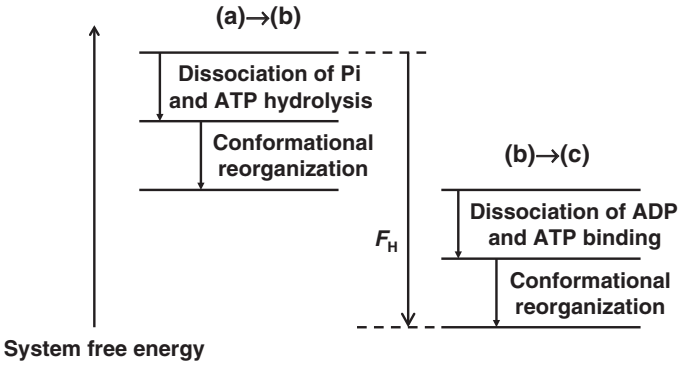

Fig. 3.16 Changes in the system free energy during the 120° rotation of the γ subunit. "ATP hydrolysis" means the hydrolysis within β_{DP}. "Conformational (structural) reorganization" means that of the $\alpha_3\beta_3\gamma$ complex. The system free energy reduces by the free-energy change upon the ATP hydrolysis in aqueous solution, F_H. (F_H is the free-energy decrease occurring when one ATP molecule is hydrolyzed in aqueous solution.)

The absolute value of the SE of each sub-complex in Fig. 3.14c is in the order, sub-complex II < sub-complex I < sub-complex III, whereas that in Fig. 3.14a is in the order, sub-complex III < sub-complex II < sub-complex I. The changes in the system free energy (SFE) during the 120° rotation are illustrated in Fig. 3.16. Though the overall conformations before and after the 120° rotation are the same, one ATP molecule is hydrolyzed in aqueous solution: The SFE becomes lower by the free-energy change upon the APT hydrolysis in aqueous solution, F_H.

Our conclusion is that the nonuniform packing efficiency in the $\alpha_3\beta_3\gamma$ complex and the water-entropy effect arising from the translational displacement of water molecules induce the rotation of the γ subunit during the ATP hydrolysis cycle. It may be worthwhile for the readers to see Sect. 3.6.7 in which the rotational mechanism is revisited, before going on to Sect. 3.5.5.

3.5.5 Effect of Direct Interaction Between Subunits

A tight packing leads to a decrease in the intramolecular energy by van der Waals and electrostatic attractive interactions among the protein atoms. We note, however, that the tight packing leads to a loss of attractive interactions with water molecules, giving rise to an increase in the protein-water interaction energy, the so-called dehydration penalty. The dehydration penalty is much larger than the intramolecular-energy decrease, and even when the energy decrease due to the structure reorganization of water is taken into account, the net change in energy can be positive. It has been suggested that the rotation is induced by the

electrostatic interaction between Arg and Lys residues on the protruding portion of the γ subunit and negatively charged residues of the β subunit, known as the DELSEED motif [50]. As explained above, however, such an energetic component can hardly be a principal factor inducing the rotation. In fact, it has experimentally been shown that the rotation is not influenced by the mutation of residues in the DELSEED motif to Ala [51]: The electrostatic interaction between the γ and β subunits plays no significant roles for the rotation.

Strikingly, it has been shown in a recent experiment [52] that the three β subunits in the $\alpha_3\beta_3$ complex (i.e., *without* the γ subunit) undergo cyclic conformational changes in the same rotary direction as in the $\alpha_3\beta_3\gamma$ complex: In the presence of ATP, only one of the three β subunits takes open conformation. When the open-to-closed transition occurs at this β subunit, the opposite closed-to-open transition occurs simultaneously at its counterclockwise neighbor β subunit. This experimental result clearly indicates that the rotation mechanism is programmed in the $\alpha_3\beta_3$ complex itself. The rotation of the γ subunit in the case of the $\alpha_3\beta_3\gamma$ complex cannot be induced by the direct interaction between the γ and β subunits.

3.6 Functional Rotation of AcrB

The polytopic inner membrane protein AcrB, periplasmic adaptor protein AcrA, and outer membrane channel TolC form the *Escherichia coli* AcrA–AcrB–TolC tripartite complex [6, 53–56]. The complex is capable of extruding a variety of drugs and considered to be a good model for multidrug efflux pumps. AcrB, which is in charge of the principal part of pumping drugs out of the cell from the inner membrane or periplasm through the TolC channel as illustrated in Fig. 3.17, is a homotrimer with a triangular-prism shape. Each protomer of AcrB comprises the transmembrane (TM), porter, and drug-efflux domains. As shown in Fig. 3.18, the three protomers take three distinct structures which are in access (A), binding (B), and extrusion (E) states along the drug transport cycle, respectively. A "functionally rotating" picture has been proposed for the transport of drugs by AcrB [54–56]. In this picture, each protomer exhibits a sequential conformational change, (A, B, E)→(B, E, A)→(E, A, B)→(A, B, E), by utilizing proton binding and dissociation (i.e., so-called proton motive force). A recent MD simulation study [57] has suggested that a single proton binds to Asp408 in the TM domain, the proton-binding site, in one protomer and the proton translocation stoichiometry is a single proton per step (e.g., (A, B, E)→(B, E, A)) in the trimer.

As observed in Fig. 3.17, the porter and drug-efflux domains are immersed in water but the TM domain is immersed in nonpolar chains of lipid molecules. These nonpolar chains also act as "solvent" (see Sect. 3.6.2). In this section, we describe the following developments on the functional-rotation mechanism of AcrB [6]: Significant nonuniformity is found in the packing efficiency of AcrB and this nonuniformity is shown to play pivotal roles through the solvent-entropy effect; it is argued how proton binding and dissociation is coupled with the functional rotation; and the reason why the AcrB proteins have to form a trimer is

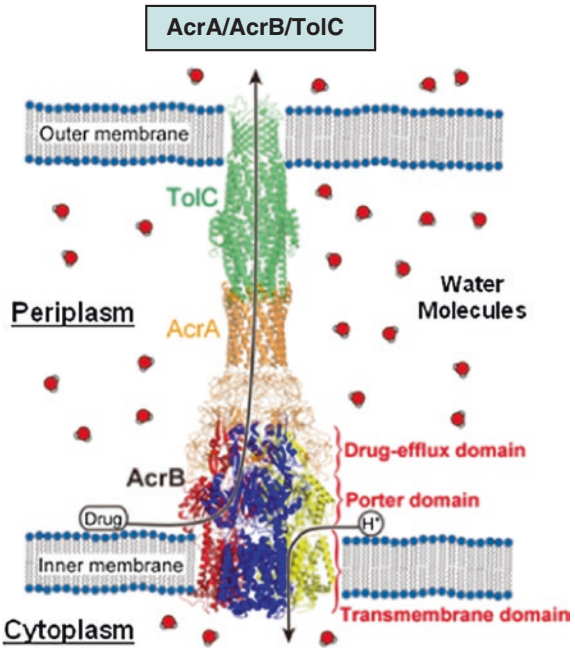

Fig. 3.17 Schematic diagram of AcrA–AcrB–TolC tripartite complex. This figure is drawn using PyMOL

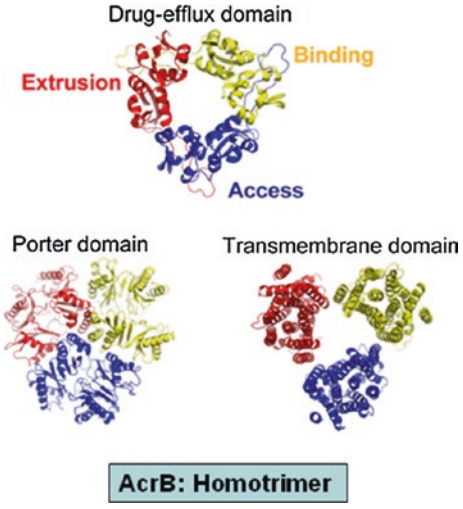

Fig. 3.18 Ribbon representation of the three domains of the protomers viewed from the top. "Access (*blue*)," "binding (*yellow*)," and "extrusion (*red*)" represent the protomers in three different states. This figure is drawn using PyMOL

clarified. The similarities to the rotation mechanism of F_1-ATPase considered in Sect. 3.5 are also discussed from a thermodynamic point of view. Unlike in the case of F_1-ATPase, there is essentially no experimental information on the functional rotation of AcrB. Hence, the discussion given is somewhat speculative but fairly sound when it is judged from a physical viewpoint.

3.6.1 Conformational Change of AcrB During One Cycle

The protomers in three different structures are referred to as protomers A (access), B (binding), and E (extrusion), respectively. A drug is ready to be inserted into protomer A, a drug is accommodated in protomer B, and a drug has been extruded from protomer E [54–56]. One cycle represented by the 120° rotation, (A, B, E)→ (B, E, A), can be described as follows. The aqueous solutions where the proton concentrations are higher and lower are referred to as higher-concentration and lower-concentration sides (i.e., periplasm and cytoplasm), respectively. A single proton is transferred from the higher-concentration side to the lower-concentration one per cycle. When Asp408 with no proton bound is exposed to the higher-concentration side, proton binding occurs because it leads to a decrease in the system free energy (SFE). On the other hand, when Asp408 with a proton bound is exposed to the lower-concentration side, proton dissociation occurs because it also leads to a decrease in the SFE (see Sect. 3.1). Hereafter, we refer to proton binding and dissociation as "proton action".

As shown in Sects. 3.3 and 3.4, when a drug is inserted into the porter domain of one of the protomers in AcrB, it can be stabilized within a cavity without contacting the protomer inner surface. Therefore, it is reasonable to assume that the drug insertion has very little effect on the structural properties of AcrB. Likewise, the drug release has also very little effect on them. As a matter of fact, we have tested two crystal structures of AcrB [6]. A drug is bound to protomer B in one of the structures, whereas no drug is bound in the other. Nevertheless, the theoretical results obtained using the two structures are qualitatively the same (the quantitative differences observed may have arisen from the different resolutions of the structural data).

Let us consider a trimer conformation, conformation 1 shown in Fig. 3.19a, where a proton is bound to none of the three protomers. The three protomers should share the same structure in conformation 1. In the absence of proton action, this conformation remains unchanged once it is reached, because it is the most stable. In the presence of proton action, when the proton binding sites are exposed to the higher-concentration side, proton first binds to one of the protomers referred to as protomer E (see conformation 2 shown in Fig. 3.19b). The trimer conformation is then perturbed, being changed toward a different, the most stable one (conformation 3 shown in Fig. 3.19c). The most stable trimer conformations before and after the proton binding are different from each other. In other words, the trimer conformation is reorganized to lower the SFE. The protomers next to protomer E in the clockwise and counterclockwise directions (when viewed from the upper side) are referred to as protomers B and A, respectively. We assume for conformation 3 that there are no open routes of proton transfer for both of the two sides in protomer E and only Asp408 of protomer B is exposed to the higher-concentration side. It follows that proton binding to protomer E persists and the next event occurring is proton binding to protomer B (conformation 4 shown in Fig. 3.19d). The trimer conformation is perturbed by the proton

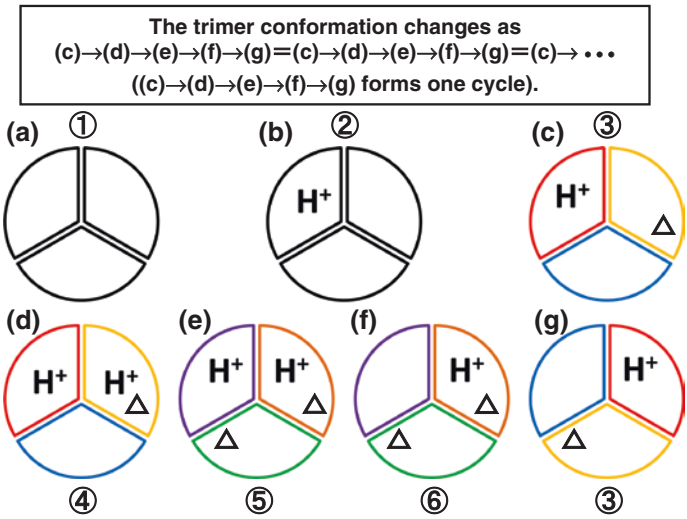

Fig. 3.19 Conformations of AcrB. Protomers A, B, E, A′, B′, and E′ are drawn in *blue*, *yellow*, *red*, *green*, *orange*, and *purple*, respectively. A different color represents a different structure. The open triangle denotes a drug molecule. **a** Conformation 1: No proton is bound to AcrB. **b** Conformation 2: Right after a proton binds to one of the protomers. **c** Conformation 3: After reorganization of AcrB conformation. **d** Conformation 4: Right after a proton binds to protomer B. **e** Conformation 5: After reorganization of AcrB conformation. **f** Conformation 6: Right after a proton dissociates from protomer E′. **g** Conformation 7: After reorganization of AcrB conformation. Conformations 3 and 7 are the same.

binding, being changed toward a different, the most stable one (conformation 5 shown in Fig. 3.19e). The protomers in Fig. 3.19e are referred to as protomers A′, B′, and E′, respectively. We assume that the route of proton transfer in protomer E′ now becomes open to the lower-concentration side: The proton dissociates from protomer E′ (conformation 6 shown in Fig. 3.19f). The trimer conformation is perturbed by the proton dissociation, being changed towards a different, the most stable one: It is conformation 3 shown in Fig. 3.19g. One cycle is thus completed [6]. The most stable conformation of the trimer is successively modified by the proton action. In Fig. 3.19c, the structures of the two protomers colored in yellow and blue are different. The reason for this is as follows. Let us consider the two edges of a protomer in Fig. 3.19a, each of which forms the interface with an edge of one of the other two protomers. Since the two edges possess different structures, their structural changes caused by proton binding influence the other two protomers in different ways.

In summary, the trimer conformation changes as (c)→(d)→(e)→(f)→(g) = (c) in Fig. 3.19. When drugs are present, a drug is bound to protomer B (yellow) in (c). A drug is inserted upon the proton binding, and in (e) drugs are bound to protomers A′ (green) and B′ (orange). Extrusion of a drug occurs upon the proton dissociation, and in (g) a drug is bound in protomer B (yellow).

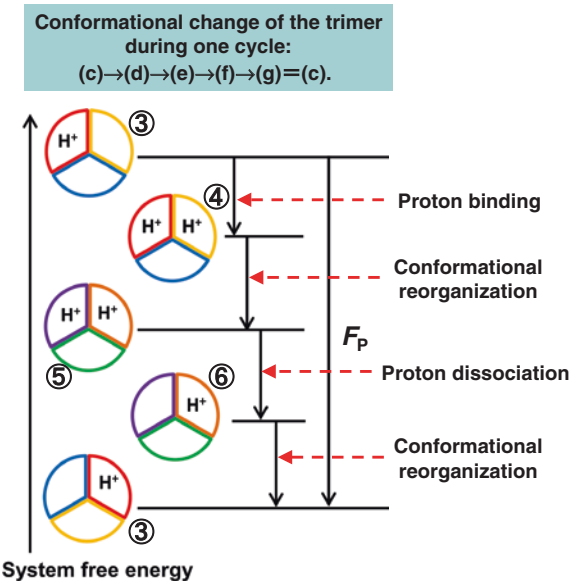

Fig. 3.20 Changes in the system free energy accompanying the conformational changes of the trimer (c)→(d)→(e)→(f)→(g) = (c) (also see Fig. 3.19). Protomers A, B, E, A′, B′, and E′ are drawn in *blue*, *yellow*, *red*, *green*, *orange*, and *purple*, respectively. A different color represents a different structure. The decrease in system free energy in one cycle is F_P

The net decrease in system free energy in each cycle is F_P as illustrated in Fig. 3.20. F_P is $\sim -8k_BT$ ($T = 298$ K) (~ -20 kJ/mol) [6]. $-8k_BT$ results from an increase of $\sim 1.7k_B$ in system entropy and a decrease of $\sim -6.5k_BT$ in system energy [6]. The entropic increase arises from the transfer of one proton from the higher-concentration side to the lower-concentration one. The energetic decrease is ascribed to the transfer of a positive charge along the electrostatic-potential gradient.

3.6.2 Model and Theory

A water molecule is modeled as a hard sphere with $d_S = 0.28$ nm in which a point dipole and a point quadrupole of tetrahedral symmetry are embedded [58, 59] ($\rho_S d_S^3 = 0.7317$). The porter and drug-efflux domains of each protomer are immersed in this model water. For the TM domain, nonpolar chains of lipid molecules forming the solvent possess not only the translational entropy (TE) but also the orientational (rotational) and vibrational entropies. As in the case of water [60, 61], the TE contribution is the principal component in the solute solvation (i.e., solvent-entropy change upon solute insertion). This is because upon solute insertion the reduction of orientational and vibrational freedoms occurs only for the solvent near the solute but that of translational freedom reaches the

whole solvent in the system. Therefore, for the TM domain, the entropic effect is ascribed primarily to the translational displacement of CH_2, CH_3, and CH groups constituting the nonpolar chains. These groups can be modeled as neutral hard spheres. Further, we note that a membrane is immersed in water. When a membrane protein takes a structure with larger EV, the membrane also generates larger EV for water molecules. Thus, water also acts as the solvent. Hence, the TM domain of each protomer is assumed to be immersed is bulk solvent comprising neutral hard spheres whose diameter and packing fraction are set at those of water. This hard-sphere solvent was shown to provide a good model of the nonpolar environment in our earlier work dealing with a membrane protein [62].

We adopt a structure model of AcrB obtained by X-ray crystallography for (c) of Fig. 3.19 (PDB CODE: 2GIF) [55]. No drug is bound to AcrB in this model. The root mean square deviation (RMSD) for C_α atoms is 0.211 nm between the structures of protomers A and B, 0.309 nm between those of protomers A and E, and 0.310 nm between those of protomers B and E. There are only slight structural differences among the three protomers. Only the structure of protomer E is significantly different, but the difference is still quite small. We have tested a different structure model in which a drug is bound to its protomer B and verified that the results obtained change only quantitatively and the conclusions drawn are not altered.

The solvent-entropy effect is crucially important. The solvation entropy plus the conformational (protein intramolecular) entropy and the solvation energy plus the conformational energy of the trimer can be considered to remain essentially constant during each cycle irrespective of the number of protons bound, one or two. This is because these thermodynamic quantities are orders of magnitude larger than the values described above, $1.7k_B$ and $-6.5k_BT$, respectively. How about these thermodynamic quantities of each protomer? As described above, there are only slight structural differences among protomers A, B, and E. We note that the solvation entropy is quite sensitive to a structural change of a protein. Even when the differences in the protein structure are slight, those in the solvation entropy are significant. For example, the root mean square deviation (RMSD) for C_α atoms between protomers A and B, which is as small as 0.211 nm, causes the difference in the solvation entropy reaching $300k_B$. Though the solvation entropy of the trimer remains essentially constant, the solvation entropies of the three protomers are considerably different from one another.

We analyze the packing efficiency of each protomer [6]. We decompose each protomer into three portions: those within the TM, porter, and drug-efflux domains, respectively. The portions within the three domains are referred to as portions T, P, D, respectively ("T," "P," and "D" denote the TM, porter, and drug-efflux domains, respectively). Let ${S_I}^M$ ($I = $ A, B, E; $M = $ T, P, D) denote the solvation entropy of portion M of protomer I. Smaller $|{S_I}^M|$ implies that the backbone and side chains of the portion are more efficiently (closely) packed.

We also analyze the packing efficiency of the interface (i.e., tightness of the interface packing) between two protomers [6]. The decomposition of each protomer into the three portions is again adopted. $\Delta {S_{IJ}}^M$ is defined as "$\Delta {S_{IJ}}^M = {S_{IJ}}^M - ({S_I}^M + {S_J}^M)$, $(I, J) = $ (A, B), (A, E), (B, E), $M = $ T, P, D" where ${S_{IJ}}^M$ is the solvation entropy of the pair of "portion M of protomer I and portion M of protomer J" taken from the trimer,

and $S_I{}^M$ and $S_J{}^M$, respectively, are the solvation entropies of "portion M of protomer I" and "portion M of protomer J" obtained simply by separating them with their structures kept unchanged. $\Delta S_{IJ}{}^M$ is positive because the overlaps of EVs occur upon the contact of the two portions. There are interfaces between portions within drug-efflux and porter domains, in which case we define $\Delta S_{IJ}{}^{\mathrm{PD}}$ as "$\Delta S_{IJ}{}^{PD} = S_{IJ}{}^{PD} - (S_I{}^P + S_J{}^D)$, $(I, J) = (\mathrm{A}, \mathrm{E}), (\mathrm{B}, \mathrm{A}), (\mathrm{E}, \mathrm{B})$," where $S_{IJ}{}^{\mathrm{PD}}$ is the solvation entropy of the pair of "portion P of protomer I and portion D of protomer J" taken from the trimer. Larger $\Delta S_{IJ}{}^M$ or $\Delta S_{IJ}{}^{\mathrm{PD}}$ implies that the interface between the two portions is more efficiently packed. Smaller $|S_I{}^M|$, larger $\Delta S_{IJ}{}^M$, and larger $\Delta S_{IJ}{}^{\mathrm{PD}}$ are more favorable with respect to the solvent entropy. We emphasize the following:

> For the trimer to maintain its high stability, $\Delta S_{IJ}{}^M$ and $\Delta S_{IJ}{}^{PD}$ must be sufficiently large for all pairs of (I, J) and all M.

In calculating the solvation entropy, we employ the ADIET-MA hybrid (see Sect. 2.6) for water and the RSIET-MA (RSIET denotes "radial-symmetric integral equation theory" [63]) hybrid for the hard-sphere solvent [62].

3.6.3 Nonuniform Packing Efficiency in AcrB

Our findings [6] can be summarized as follows. Within the drug-efflux domain, the differences among the three protomers in the packing efficiency are relatively small. Within the porter domain, protomer B is overall less closely packed than the other two protomers (see the right diagram in Fig. 3.22b) probably due to the presence of an accommodation space for a drug. Within the TM domain, protomer E is overall more closely packed (see the right diagram in Fig. 3.22a), which is attributable to proton binding. Overall, the interfaces between portions within the drug-efflux domain are tightly packed. This is because part of each portion is penetrating into the adjacent portion (see Fig. 3.21). The tight packing through the penetration within the drug-efflux domain makes a substantial contribution to the stability of the trimer. It can be assumed for simplicity that any of the portions within the drug-efflux domain preserves the same structure during each cycle due to the tight packing [6].

Within each domain, the packing efficiencies of the three interfaces are not significantly different from one another. This is suggestive that impartial, the closest possible packing of all of the three interfaces is crucial for the maintenance of high stability of the trimer.

3.6.4 Conformational Reorganization Induced by Proton Binding or Dissociation

A TM domain comprises 12 α-helices, TM1-TM12. A proton binds to Asp408 in TM4 [57]. We have found that upon this binding the overall packing efficiency of

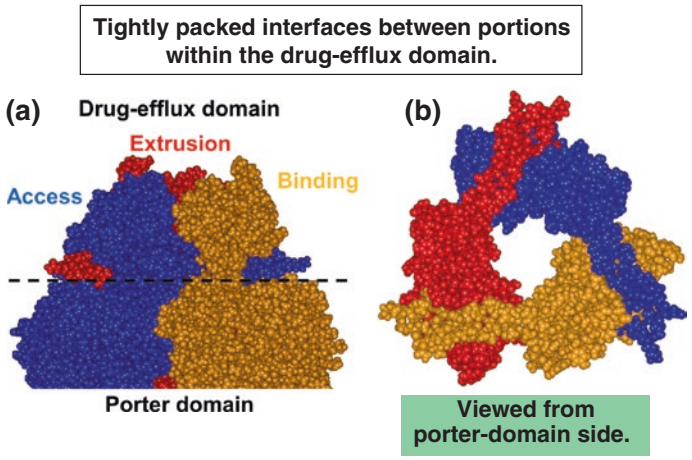

Fig. 3.21 **a** Space-filled representation of drug-efflux (*above* the *broken line*) and porter (*below* the *broken line*) domains of protomers A (access: *blue*) and B (binding: *yellow*). **b** Space-filled representation of drug-efflux domain of protomers A (access: *blue*), B (binding: *yellow*), and E (extrusion: *red*) viewed from porter domain side. This figure is drawn using the DS visualizer 2.5

the TM domain becomes higher. Inversely, upon the proton dissociation, the opposite changes occur, leading to lower overall packing efficiency. The structural change of the TM domain accompanying proton binding or dissociation becomes a trigger of conformational reorganization of the trimer. More detailed information on the conformational reorganizations caused by proton binding and dissociation are included in the conformational transitions (a)→(c) and (c)→(a) in Fig. 3.19, respectively, and it is illustrated in Fig. 3.22. The left diagrams in black of Fig. 3.22 correspond to (a) of Fig. 3.19, and the right diagrams in color of Fig. 3.22 correspond to (c) of Fig. 3.19. The three protomers share the same structure in the left diagrams. The solvation entropy of the trimer in the left diagrams is approximately equal to that in the right diagrams. $|S_I{}^M|$ and $\Delta S_{IJ}{}^M$ in the left diagrams are calculated by assuming that the closest possible packing properties are achieved at the three interfaces within the porter and TM domains and they therefore remain unchanged. In Fig. 3.22b, for example, $(60k_B+270k_B)/3=110k_B$ and $(80k_B+70k_B+60k_B)/3=70k_B$. There are also packed interfaces between protomers within the drug-efflux and porter domains. The values of $\Delta S_{IJ}{}^M$ for the yellow-red, yellow-blue, and red-blue interfaces are $90k_B$, 80 k_B, and $70k_B$, respectively (not shown in Fig. 3.22).

On the basis of the information provided in Fig. 3.22, we make the following propositions [6]:

I. First, the change caused by proton binding to a protomer is discussed. For the portions within the TM domain (see Fig. 3.22a), the following conformational reorganization occurs: (i) $|S_I{}^T|$ of this protomer decreases by $130k_B$; (ii) $|S_I{}^T|$ of the protomer next to it in the clockwise direction increases by $80k_B$; and (iii) $|S_I{}^T|$ of the protomer next to it in the counterclockwise direction increases by $50k_B$. The decrease mentioned in (i) is consistent with the increased overall packing

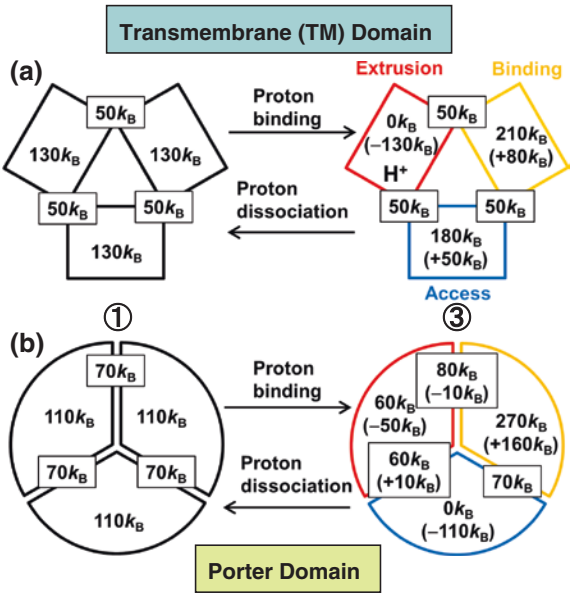

Fig. 3.22 Information on the structural reorganizations caused by proton binding and dissociation. The numbers given denote the *relative* values of $|S_I{}^M|$, and those within the parentheses represent their changes due to conformational reorganization of the trimer caused by proton binding. Those within rectangles denote the values of $\Delta S_{IJ}{}^M$. Smaller $|S_I{}^M|$ implies that the backbone and side chains of the portion are more efficiently (closely) packed. Larger $\Delta S_{IJ}{}^M$ implies that the interface between the two portions is more efficiently packed. Protomers A, B, and E are drawn in *blue*, *yellow*, and *red*, respectively. A different color represents a different structure

efficiency for this protomer within the TM domain explained above. For the portions within the porter domain (see Fig. 3.22b), the following conformational reorganization occurs: (iv) $|S_I{}^P|$ of this protomer decreases by $50k_B$; (v) $|S_I{}^P|$ of the protomer next to it in the clockwise direction increases by $160k_B$; and (vi) $|S_I{}^P|$ of the protomer next to it in the counterclockwise direction decreases by $110k_B$. The decrease mentioned in (i) induces an increase in overall packing efficiency for this protomer within the porter domain, leading to the decrease mentioned in (iv). The increase mentioned in (v) implies that the protomer becomes less closely packed, which is consistent with the generation of accommodation space for a drug. This increase induces the decrease mentioned in (vi). The packing properties of the three interfaces also undergo the changes illustrated in Fig. 3.22b.

II. Second, the change caused by proton dissociation from a protomer is discussed. For the portions within the TM domain (see Fig. 3.22a), the following conformational reorganization occurs: (vii) $|S_I{}^T|$ of this protomer increases by $130k_B$; (viii) $|S_I{}^T|$ of the protomer next to it in the clockwise direction decreases by $80k_B$; and (ix) $|S_I{}^T|$ of the protomer next to it in the counterclockwise direction decreases by $50k_B$. The increase mentioned in (vii) is consistent with the decreased overall packing efficiency for this protomer within the TM domain

described above. For the portions within the porter domain (see Fig. 3.22b), the following conformational reorganization occurs: (x) $|S_I{}^{\mathrm{P}}|$ of this protomer increases by $50k_{\mathrm{B}}$; (xi) $|S_I{}^{\mathrm{P}}|$ of the protomer next to it in the clockwise direction decreases by $160k_{\mathrm{B}}$; and (xii) $|S_I{}^{\mathrm{P}}|$ of the protomer next to it in the counter-clockwise direction increases by $110k_{\mathrm{B}}$. The decrease mentioned in (xi) implies that the protomer becomes more closely packed, which is consistent with the disappearance of accommodation space for a drug. The packing properties of the three interfaces also undergo the changes illustrated in Fig. 3.22b.

3.6.5 Physical Picture of Functional-Rotation Mechanism

We now discuss the physical meaning of the propositions made above. It is assumed that the propositions are always applicable to the conformational reorganization accompanying proton binding or dissociation. Our interpretation of the functional rotation can be illustrated in Fig. 3.23. The left, middle, and right conformations in this figure correspond to those of (c), (e), and (g) in Fig. 3.19, respectively. The upper three diagrams are for the porter domain and the lower three diagrams are for the TM domain. The numbers given denote the values of $|S_I{}^{M}|$ for the three portions of each protomer and those within parentheses denote the changes caused by proton binding (middle) or proton dissociation (right). The physical essence of the functional-rotation mechanism proposed is the following [6]:

> When a proton binds to or dissociates from a protomer, the packing properties of this protomer and its two interfaces are perturbed on the whole in the direction that the solvent entropy is lowered. The packing properties of the other two protomers are then reorganized so that the closely packed interfaces can be recovered and the solvent-entropy loss can be compensated. The solvent entropy is thus kept almost constant.

When a proton binds to protomer B as (left)→(middle) in Fig. 3.23, its structure is perturbed in the direction that the solvent entropy is lowered. This can be understood as follows. The protomer after the structural perturbation is referred to as protomer B′. $|S_{\mathrm{B}'}{}^{\mathrm{T}}|$ and $|S_{\mathrm{B}'}{}^{\mathrm{P}}|$ are lower than $|S_{\mathrm{B}}{}^{\mathrm{T}}|$ and $|S_{\mathrm{B}}{}^{\mathrm{P}}|$, respectively, which implies that the backbone and side chains are more closely packed in protomer B′ than in protomer B. It should be noted, however, that the closer packing followed by reduction of the EV gives rise to looser packing of the B-E and B-A interfaces. Within the TM domain, proton binding would induce not only a solvent-entropy gain of $130k_{\mathrm{B}}$ arising from the closer packing of protomer B but also a solvent-entropy loss of $100k_{\mathrm{B}}$ ($= 50k_{\mathrm{B}} + 50k_{\mathrm{B}}$: "$50k_{\mathrm{B}}$ and $50k_{\mathrm{B}}$" come from the values of $\Delta S_{IJ}{}^{M}$ for the yellow-red and yellow-blue interfaces within the TM domain) at most caused by the looser packing of the interfaces. Within the porter domain, proton binding tries to induce a solvent-entropy loss of $320k_{\mathrm{B}}$ ($= 80k_{\mathrm{B}} + 70k_{\mathrm{B}} + 90k_{\mathrm{B}} + 80k_{\mathrm{B}}$: "$80k_{\mathrm{B}}$ and $70k_{\mathrm{B}}$" come from the values of $\Delta S_{IJ}{}^{M}$ for the yellow-red and yellow-blue interfaces within the porter domain; "$90k_{\mathrm{B}}$ and $80k_{\mathrm{B}}$" come from the values of $\Delta S_{IJ}{}^{M}$ for the yellow-red and yellow-blue interfaces between the drug-efflux and porter domains) at most originating from the looser packing of the interfaces as well as a solvent-entropy gain of $50k_{\mathrm{B}}$ brought

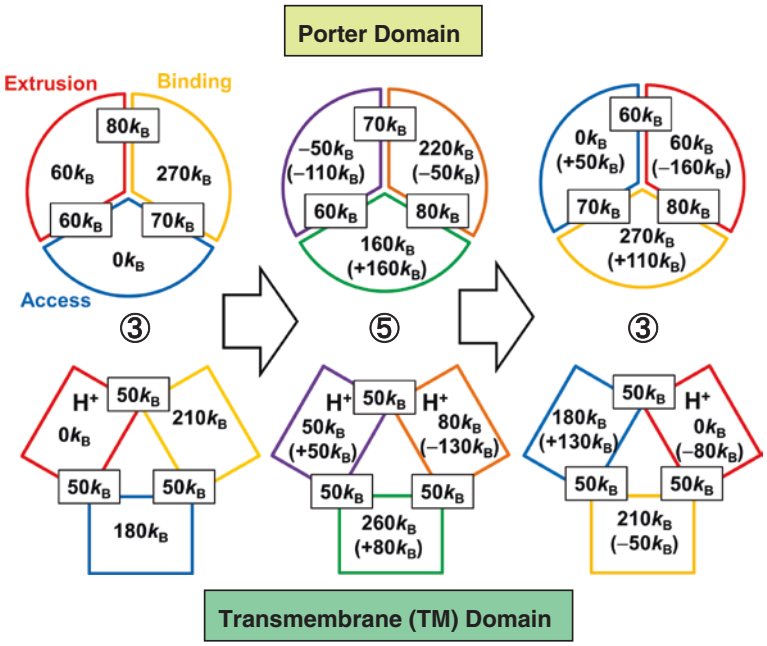

Fig. 3.23 Interpretation of the functional rotation. The numbers given denote the *relative* values of $|S_I{}^M|$, and those within the parentheses represent their changes due to conformational reorganization of the trimer caused by proton binding or dissociation. Those within rectangles denote the values of $\Delta S_{IJ}{}^M$. Smaller $|S_I{}^M|$ implies that the backbone and side chains of the portion are more efficiently (closely) packed. Larger $\Delta S_{IJ}{}^M$ implies that the interface between the two portions is more efficiently packed. The left, middle, and right conformations (they are referred to as (*left*), (*middle*), and (*right*), respectively) correspond to conformations 3, 5, and 7 (see Fig. 3.19), respectively. Protomers A, B, E, A′, B′, and E′ are drawn in *blue*, *yellow*, *red*, *green*, *orange*, and *purple*, respectively. A different color represents a different structure

by the closer packing of protomer B. The net gains and losses are $180k_B$ and $420k_B$, respectively. $420k_B$ is the maximum value, but it is probable that the net loss is larger because even slightly looser interface packing causes a significantly large decrease in solvent entropy. Taken together, proton binding to protomer B would induce a significantly large loss of solvent entropy. This loss is compensated with the structural reorganization of the other two protomers primarily to recover the close packing of the interfaces.

When a proton dissociates from protomer E′ shown in the middle of Fig. 3.23, the structure of this protomer is perturbed in the direction that the solvent entropy is lowered. This can readily be understood. The protomers before and after the structural perturbation are protomers E′ and A, respectively. $|S_A{}^T|$ and $|S_A{}^P|$ are higher than $|S_{E'}{}^T|$ and $|S_{E'}{}^P|$, respectively, which implies that the backbone and side chains are less closely packed in protomer A than in protomer E′. In this case, the two interfaces are already packed with sufficient tightness and not significantly

affected by the proton dissociation. The solvent-entropy loss is compensated with the structural reorganization of the other two protomers which still retains the close packing of the interfaces.

Our physical picture is not deteriorated at all even if the energetic component (i.e., sum of conformational energy and hydration energy) is taken into account. By performing a similar analysis based on the energetic component as well as the solvation entropy, we will reach the following conclusion: When a proton binds to or dissociates from a protomer, the structural properties of this protomer and its two interfaces are perturbed on the whole in the direction that the system free energy (SFE) becomes higher; hence, the structural properties of the other two protomers are reorganized so that the SFE increase can be compensated and the SFE is kept almost constant.

3.6.6 Significance of Trimer Formation

The solvation entropies of protomers A, B, and E are $-36{,}700k_B$, $-37{,}000k_B$, and $-36{,}400k_B$, respectively. An isolated protomer cannot realize the functional rotation "A→B→E→A" by itself, because "A→B" and "E→A" would cause a prohibitively large loss of solvent entropy, $300k_B$. In the trimer, however, the solvent-entropy loss caused by a protomer is *always* cancelled out by the solvent-entropy gain brought by the other two protomers. As a result, each protomer accomplishes the functional rotation using the SFE decrease arising from the transfer of only a single proton, which is as small as F_P, with no free-energy barriers. The trimer formation thus provides a judicious method for expressing a high function with the consumption of only very small free energy.

Even if the energetic component is taken into account, the basic framework is essentially the same. The description is altered simply as follows: By forming a trimer, any SFE increase caused by a protomer is always cancelled out by the SFE decrease brought by the other two protomers. Still, we believe that the changes in SFE originate primarily from those of solvent entropy. It is probable that the closest overall packing is achievable when three (e.g., neither two nor four) protomers aggregate: For AcrB, the polyatomic structure of a protomer is constructed so that this feature can be conferred upon it.

3.6.7 Comparison Between AcrB and F_1-ATPase

Here, the rotational mechanism of the $\alpha_3\beta_3\gamma$ complex (i.e., F_1-ATPase) [3, 4] is recapitulated in a different way. We refer to the binding of ATP, hydrolysis of ATP into ADP and Pi, and dissociation of ADP and Pi as "ATP action". Without the ATP action, once the $\alpha_3\beta_3\gamma$ complex reaches the most stable conformation, this conformation does not change any more. In Sect. 3.5, the complex was

decomposed into three portions. It was found that in the most stable conformation the packing efficiencies of the three portions are substantially different from one another. Due to the ATP action, the most stable conformation is perturbed and the conformational reorganization of the complex occurs to reach a different, the most stable conformation. The physical essence is the following: When the structure of one of the three portions is perturbed in the direction that a solvent-entropy loss is caused, the structures of the other two portions are reorganized to compensate the loss (i.e., when one of the three portions is less closely packed, the other two portions are more closely packed). It is no wonder that the cyclic conformational changes occur even in the $\alpha_3\beta_3$ complex (i.e., *without* the γ subunit) [52] just as in AcrB. In the presence of the γ subunit, the conformational reorganization induces its rotation (120° rotation per ATP hydrolysis cycle). The rotation is accomplished by the SFE decrease arising from the hydrolysis of only a single ATP molecule, which is as small as F_H. Thus, F_1-ATPase and AcrB share physically the same rotational mechanism.

References

1. K. Amano, T. Yoshidome, M. Iwaki, M. Suzuki, M. Kinoshita, J. Chem. Phys. **133**, 045103 (2010)
2. K. Amano, H. Oshima, M. Kinoshita, J. Chem. Phys. **135**, 185101 (2011)
3. T. Yoshidome, Y. Ito, M. Ikeguchi, M. Kinoshita, J. Am. Chem. Soc. **133**, 4030 (2011)
4. T. Yoshidome, Y. Ito, N. Matubayasi, M. Ikeguchi, M. Kinoshita, J. Chem. Phys. **137**, 035102 (2012)
5. K. Hollenstein, R.J.P. Dawson, K.P. Locher, Curr. Opin. Struct. Biol. **17**, 412 (2007)
6. H. Mishima, H. Oshima, S. Yasuda, M. Kinoshita, J. Phys. Chem. B **119**, 3423 (2015)
7. S.M. Block, Biophys. J. **92**, 2986 (2007)
8. E. Hirakawa, H. Higuchi, Y.Y. Toyoshima, Proc. Natl. Acad. Sci. U.S.A. **99**, 2533 (2000)
9. J.L. Ross, M.Y. Ali, D.M. Warshaw, Curr. Opin. Cell Biol. **20**, 41 (2008)
10. T. Yanagida, S. Esaki, A.H. Iwane, Y. Inoue, A. Ishijima, K. Kitamura, H. Tanaka, M. Tokunaga, Phil. Trans. R. Soc. Lond. B **355**, 441 (2000)
11. T. Okada, H. Tanaka, A.H. Iwane, K. Kitamura, M. Ikebe, T. Yanagida, Biochem. Biophys. Res. Commun. **354**, 379 (2007)
12. Y. Okada, N. Hirokawa, Science **283**, 1152 (1999)
13. K. Kitamura, M. Tokunaga, A.H. Iwane, T. Yanagida, Nature **397**, 129 (1999)
14. K. Kitamura, M. Tokunaga, S. Esaki, A.H. Iwane, T. Yanagida, Biophysics **1**, 1 (2005)
15. D. Beglov, B. Roux, J. Chem. Phys. **103**, 360 (1995)
16. M. Ikeguchi, J. Doi, J. Chem. Phys. **103**, 5011 (1995)
17. M. Kinoshita, J. Chem. Phys. **116**, 3493 (2002)
18. T. Kodama, Physiol. Rev. **65**, 467 (1985)
19. T. Katoh, F. Morita, J. Biochem. **120**, 189 (1996)
20. P. Coureux, A.L. Wells, J. Menetrey, C.M. Yengo, C.A. Morris, H.L. Sweeney, A. Houdusse, Nature **425**, 419 (2003)
21. P. Coureux, H.L. Sweeney, A. Houdusse, EMBO J. **23**, 4527 (2004)
22. R. Ananthakrishnan, A. Ehrlichter, Int. J. Biol. Sci. **3**, 303 (2007)
23. H. Noji, R. Yasuda, M. Yoshida, K. Kinosita Jr., Nature **386**, 299 (1997)
24. A.L. Horwich, W.A. Fenton, E. Chapman, G.W. Farr, Annu. Rev. Cell Dev. Biol. **23**, 115 (2007)
25. T.K. Chaudhuri, V.K. Verma, A. Maheshwari, Prog. Biophys. Mol. Biol. **99**, 42 (2009)

26. S. Tanaka, Y. Kawata, G. Otting, N.E. Dixon, K. Matsuzaki, M. Hoshino, Biochim. Biophys. Acta **1804**, 866 (2010)
27. H. Mishima, H. Oshima, S. Yasuda, K. Amano, M. Kinoshita, J. Chem. Phys. **139**, 205102 (2013)
28. M.A. Seeger, K. Diederichs, T. Eicher, L. Brandstätter, A. Schiefner, F. Verrey, K.M. Pos, Curr. Drug Targets **9**, 729 (2008)
29. X.-Z. Li, H. Nikaido, Drugs **69**, 1555 (2009)
30. K.M. Pos, Biochim. Biophys. Acta **1794**, 782 (2009)
31. T. Hayashi, S. Chiba, Y. Kaneta, T. Furuta, M. Sakurai, J. Phys. Chem. B **118**, 12612 (2014)
32. F. Takagi, N. Koga, S. Takada, Proc. Natl. Acad. Sci. U.S.A. **100**, 11367 (2003)
33. W. Xu, J. Wang, W. Wang, Proteins **61**, 777 (2005)
34. K.L. Nielsen, N. Mclennan, M. Masters, N.J. Cowan, J. Bacteriol. **181**, 5871 (1999)
35. R. Hara, K. Amano, M. Kinoshita, A. Yoshimori, J. Chem. Phys. **144**, 105103 (2016)
36. A. Ward, C.L. Reyes, J. Yu, C.B. Roth, G. Chang, Proc. Natl. Acad. Sci. U.S.A. **104**, 19005 (2007)
37. L. Vaccaro, K.A. Scott, M.S.P. Sansom, Biophys. J. **95**, 5681 (2008)
38. S. Murakami, R. Nakashima, E. Yamashita, T. Matsumoto, A. Yamaguchi, Nature **443**, 173 (2006)
39. S. Murakami, Curr. Opin. Struct. Biol. **18**, 459 (2008)
40. T. Imai, N. Miyashita, Y. Sugita, A. Kovalenko, F. Hirata, A. Kidera, J. Phys. Chem. B **115**, 8288 (2011)
41. J.P. Abrahams, A.G. Leslie, R. Lutter, J.E. Walker, Nature **370**, 621 (1994)
42. D. Okuno, R. Fujisawa, R. Iino, Y. Hirono-Hara, H. Imamura, H. Noji, Proc. Natl. Acad. Sci. U.S.A. **105**, 20722 (2008)
43. H. Sieladd, H. Rennekamp, S. Engelbrecht, W. Junge, Biophys. J. **95**, 4979 (2008)
44. T. Masaike, F. Koyama-Horibe, K. Oiwa, M. Yoshida, T. Nishizaka, Nat. Struct. Mol. Biol. **15**, 1326 (2008)
45. R. Yasuda, H. Noji, K. Kinosita Jr., M. Yoshida, Cell **93**, 1117 (1998)
46. K. Adachi, K. Oiwa, T. Nishizaka, S. Furuike, H. Noji, H. Itoh, M. Yoshida, M. Kinosita Jr., Cell **130**, 309 (2007)
47. Y. Ito, M. Ikeguchi, J. Comput. Chem. **31**, 2175 (2010)
48. M.W. Bowler, M.G. Montgomery, A.G.W. Leslie, J.E. Walker, J. Biol. Chem. **282**, 14238 (2007)
49. S. Adinolfi, M. Nair, A. Politou, E. Bayer, S. Martin, P. Temussi, A. Pastore, Biochemistry **43**, 6511 (2004)
50. J. Ma, T.C. Flynn, Q. Cui, A.G.W. Leslie, J.E. Walker, M. Karplus, Structure **10**, 921 (2002)
51. K.Y. Hara, H. Noji, D. Bald, R. Yasuda, K. Kinosita Jr., M. Yoshida, J. Biol. Chem. **275**, 14260 (2000)
52. T. Uchihashi, R. Iino, T. Ando, H. Noji, Science **333**, 755 (2011)
53. V. Koronakis, A. Sharff, E. Koronakis, B. Luisi, C. Hughes, Nature **405**, 914 (2000)
54. S. Murakami, R. Nakashima, E. Yamashita, T. Matsumoto, A. Yamaguchi, Nature **443**, 173 (2006)
55. M.A. Seeger, A. Schiefner, T. Eicher, F. Verrey, K. Diederichs, K.M. Pos, Science **313**, 1295 (2006)
56. G. Sennhauser, P. Amstutz, C. Briand, O. Storchenegger, M. Grütter, PLOS Biol. **5**, e7(0106) (2007)
57. T. Yamane, S. Murakami, M. Ikeguchi, Biochemistry **52**, 7648 (2013)
58. P.G. Kusalik, G.N. Patey, J. Chem. Phys. **88**, 7715 (1988)
59. P.G. Kusalik, G.N. Patey, Mol. Phys. **65**, 1105 (1988)
60. Y. Harano, M. Kinoshita, Biophys. J. **89**, 2701 (2005)
61. M. Kinoshita, J. Chem. Phys. **128**, 024507 (2008)
62. S. Yasuda, H. Oshima, M. Kinoshita, J. Chem. Phys. **137**, 135103 (2012)
63. J.-P. Hansen, L.R. McDonald, *Theory of Simple Liquids*, 3rd edn. (Academic, London, 2006)

Chapter 4
Concluding Remarks: Mechanism of Functional Expression Common in the Molecular Machines

Abstract Let us take protein folding as an example. The initial and final states of the folding process are visually different: Protein is in unfolded and folded states, respectively. Therefore, it can readily be understood that protein folding spontaneously occurs as an irreversible process accompanying a decrease in the system free energy. On the other hand, the conformations of F_1-ATPase before and after a 120° rotation of the central subunit, for example, are the same. Nevertheless, the directed rotation occurs. Hence, in the prevailing view, this rotation process is differently treated: It is made possible by converting the free energy of ATP hydrolysis to a work, and F_1-ATPase is referred to as "molecular rotatory machine." The work is necessary for the central subunit (i.e., γ subunit) to rotate against the viscous resistance force by water. Similarly, the unidirectional movement of S1 is realized by converting the free energy of ATP hydrolysis to a work that is necessary for S1 to move against the viscous resistance force by water. We disagree with this view (also see Sect. 3.2.5) In this chapter, we argue that protein folding and the directed rotation, for example, can be treated within the same theoretical framework.

Keywords ATP-driven protein · Motor protein · Molecular machine · Irreversible process

4.1 Characteristics Common in ATP-Driven Proteins and Protein Complexes

Water forms a potential field between the myosin-F-actin, protein-chaperonin, and substrate-ABC transporter pairs, as argued in Sects. 3.2, 3.3, and 3.4, respectively. The entropic component of the field is substantial, but the energetic component is also important for a chaperonin. The field is strongly dependent on the structure and properties of the pairs. When the ATP concentration is sufficiently high and the ADP and Pi concentrations are sufficiently low, the dissociation of ADP or Pi from as well as the binding of ATP to a receptor decreases the system free energy (SFE):

M. Kinoshita, *Mechanism of Functional Expression of the Molecular Machines*, SpringerBriefs in Molecular Science, DOI 10.1007/978-981-10-1486-4_4

They unavoidably occur. The hydrolysis of ATP within the receptor accompanies a small decrease in the SFE. The occurrence of any of the ATP binding, hydrolysis, and dissociation of ADP or Pi perturbs the structure and properties of the pairs. The perturbation causes an alteration of the potential field. Through this mechanism, a variety of functions such as the unidirectional movement of myosin and insertion and release of a protein or a substrate are exhibited. In each cycle, the original configuration of myosin, chaperonin, or ABC transporter is recovered and the cycle is repeatable. One ATP molecule is hydrolyzed in each cycle for actomyosin and the SFE decreases by the free energy of ATP hydrolysis in aqueous solution, F_H (see the caption for Fig. 3.2). Two ATP molecules are hydrolyzed for an ABC transporter while seven ATP molecules are hydrolyzed for GroEL: The free-energy decreases are much larger. For the chaperonin, the free-energy decrease due to protein folding also occurs. For the ABC transporter, part of the free energy of ATP hydrolysis is consumed for the transport of a substrate against the chemical-potential gradient.

In the case of the $\alpha_3\beta_3\gamma$ complex in F_1-ATPase (see Sect. 3.5), a highly nonuniform packing structure of the complex is stabilized by the water-entropy effect. In particular, one of the sub-complexes incorporating the γ subunit with a special orientation is tightly packed. This feature is attributable to the nonuniform binding of nucleotides to the three β subunits and the twisted structure of the γ subunit (the former factor is more important). The perturbation of the packing structure by any of the ATP binding, hydrolysis, or dissociation of ADP or Pi gives rise to the reorganization of the packing structure by the water-entropy effect. The reorganization accompanies the rotation of the γ subunit. In one cycle the γ subunit rotates by 120° and the original packing structure is recovered. The SFE decreases by the free energy of ATP hydrolysis. The rotation is repeatable. The keywords could be water-entropy effect, nonuniform packing of the complex, and ATP hydrolysis cycle.

There is a general trend that only the roles of ATP are emphasized, but the functions of all those molecular machines are expressed by the cooperation of water and ATP (more specifically, an ensemble of water molecules and the ATP hydrolysis cycle). This new view is in marked contrast with the conventional one, "the unidirectional movement of S1, for instance, is realized by converting the free energy of ATP hydrolysis to a work that is necessary for S1 to move against the viscous resistance force by water" [1], which implies that water hinders the unidirectional movement and functional expression of S1.

4.2 Roles of ATP Hydrolysis Cycle and Proton Motive Force

One can readily understand that protein folding, for example, is an irreversible process accompanying a decrease in the SFE. This is because the protein conformations before and after the folding are different. By contrast, the conformations of F_1-ATPase or those of AcrB before and after the rotation are the same. Why

does the rotation occur? The answer is as follows: The rotation becomes an irreversible process thanks to the ATP or proton action [2].

In the case of F_1-ATPase, the chemical reaction,

$$\mathrm{ATP} + \mathrm{H_2O} \rightleftharpoons \mathrm{ADP} + \mathrm{Pi} + \mathrm{H^+},$$

is not in equilibrium in the aqueous solution in which F_1-ATPase is immersed. That is, the concentrations of ATP and ADP are too high and too low, respectively, and the reaction proceeds in the right direction. It proceeds, however, only with the catalyst, β subunit. ATP binds to the β subunit from the aqueous solution, hydrolysis occurs, and the products ADP and Pi are released to the aqueous solution. This hydrolysis cycle induces conformational reorganizations of the $\alpha_3\beta_3\gamma$ complex, which is accompanied by a rotation of the γ subunit. Before and after the rotation, the conformations of the $\alpha_3\beta_3\gamma$ complex are the same. Nevertheless, the rotation proceeds because it is an irreversible process accompanying a decrease in the SFE: Note that one ATP molecule has been decomposed to ADP and Pi molecules in the aqueous solution. Similar concepts are applicable to the functional expressions of actomyosin, a chaperonin, and an ABC transporter.

In the case of AcrB, the two aqueous solutions (higher-concentration and lower-concentration sides) are not in equilibrium with each other in terms of the proton concentration. Hence, the proton transfer occurs, but only through the binding to AcrB from the higher-concentration side followed by the dissociation from AcrB to the lower-concentration side [2]. This transfer induces the functional rotation. Before and after the rotation, the conformations of AcrB are the same. Nevertheless, the rotation proceeds because it is an irreversible process accompanying a decrease in the SFE: Note that one proton has transferred from the higher-concentration side to the lower-concentration one.

Thus, the change of the most stable conformation of F_1-ATPase or AcrB is made possible by the concert with an irreversible process (i.e., the chemical reaction described above or the proton transfer) [2]. Moreover, the change is repeatable because the nonequilibrium process takes place successively. The rotation of the γ subunit within F_1-ATPase or the functional rotation of AcrB does occur because it is coupled with an irreversible process.

4.3 Self-assembly and Ordering Processes

In our view, the self-assembly and ordering processes can be treated in a unified manner within the same theoretical framework. For example, protein folding and the rotation of the central subunit within F_1-ATPase are both irreversible processes accompanying a decrease in the SFE. As long as the dynamics is not considered, the mechanisms of protein folding and the rotation can be investigated using equilibrium statistical mechanics as done in this book. We emphasize that water always plays imperative roles. An important difference between protein folding and the rotation is as follows: The former is inherently an irreversible process, whereas the latter becomes irreversible only when it is coupled with the irreversible ATP hydrolysis.

4.4 Rotation of Central Subunit Within F_1-ATPase in Opposite Direction

In Sect. 3.5, Pi, ATP, and ATP ready to be hydrolyzed into ADP + Pi are bound to β_E, β_{TP}, and β_{DP}, respectively. The fundamental events are "dissociation of Pi from β_E ($\beta_E \rightarrow \beta'_E$) and hydrolysis of ATP within β_{DP} ($\beta_{DP} \rightarrow \beta_{DP}^{HO}$) accompanying a conformational change of β_{TP} ($\beta_{TP} \rightarrow \beta'_{TP}$)" and "binding of ATP to β'_E ($\beta'_E \rightarrow \beta_{TP}$) and dissociation of ADP from β_{DP}^{HO} ($\beta_{DP}^{HO} \rightarrow \beta_E$) accompanying a conformational change of β'_{TP} ($\beta'_{TP} \rightarrow \beta_{DP}$)". In one cycle, the changes of $\beta_{DP} \rightarrow \beta_E$, $\beta_{TP} \rightarrow \beta_{DP}$, and $\beta_E \rightarrow \beta_{TP}$ occur and the γ subunit rotates by 120° in a counterclockwise direction. Next, we consider F_1-ATPase in the following two cases: (1) The concentrations of ATP and ADP are too low and too high (the Pi concentration is also sufficiently high), respectively, and the chemical reaction described above proceeds in the left direction (i.e., ATP synthesis occurs); and (2) the reaction is in equilibrium. In case (1), each cycle comprises binding of ADP and Pi to a receptor in a protein or protein complex, synthesis of ATP from ADP + Pi within the receptor, and dissociation of ATP from the receptor.

In case (1), Pi, ATP, and ADP + Pi ready to be synthesized into ATP are bound to β_E, β_{TP}, and β_{DP}, respectively. The fundamental events could be "dissociation of ATP from β_{TP} ($\beta_{TP} \rightarrow \beta'_E$) and synthesis of ATP within β_{DP} ($\beta_{DP} \rightarrow \beta'_{TP}$) accompanying a conformational change of β_E ($\beta_E \rightarrow \beta^*$)" and "binding of ADP to β^* ($\beta^* \rightarrow \beta_{DP}$) and binding of Pi to β'_E ($\beta'_E \rightarrow \beta_E$) accompanying a conformational change of β'_{TP} ($\beta'_{TP} \rightarrow \beta_{TP}$)". In one cycle, the changes of $\beta_{DP} \rightarrow \beta_{TP}$, $\beta_{TP} \rightarrow \beta_E$, and $\beta_E \rightarrow \beta_{DP}$ occur and the γ subunit rotates by 120° in a clockwise direction. In case (2), the reaction rates for the right and left directions are equal: The reaction is never stopped. Therefore, the rotation sometimes occurs both in the counterclockwise and clockwise directions with the same probability: The orientation of the γ subunit just fluctuates, and the directed rotation does not take place.

Even when the ATP concentration is sufficiently high and the ADP and Pi concentrations are sufficiently low as in Sect. 3.5, the reaction rate for the left direction is not zero. Infrequently, the ATP synthesis occurs and the γ subunit rotates in the opposite direction: In fact, such opposite rotations have been observed in experiments [3, 4].

4.5 Movement of Myosin Head (S1) Along F-Actin

The binding site for ATP or ADP within S1 is located on the either right or left side of S1. This location determines which direction is right or left. We postulate in Sect. 3.2 that the movement of S1 occurs in the right direction through the changes per cycle, "black curve → red curve (upon ATP binding) → red curve (during ATP hydrolysis) → black curve (upon Pi dissociation) → black curve

(upon ADP dissociation)". Next, we consider S1 on F-actin in the two cases mentioned in Sect. 4.4.

In case (1), the changes per cycle can be "black curve → black curve (upon ADP binding) → red curve (upon Pi binding) → red curve (during ATP synthesis) → black curve (upon ATP dissociation)". Again, the movement of S1 occurs in the right direction. As discussed in Sect. 3.2.4, the switch from the black curve to the red one does occur not abruptly but rather gradually: As S1 moves along F-actin in the right direction, the potential felt by S1 continues to shift in the lower direction. Further, as the ATP hydrolysis or synthesis proceeds, the potential continues to decrease: As S1 moves along F-actin in the right direction, the potential felt by S1 continues to shift in the lower direction. These two effects should also promote the unidirectional movement of S1. One might think that even in case (2) S1 moves in the right direction by the repeated switches from one of the black and red curves to the other, which conflicts with the second law of thermodynamics. What happens in case (2)? There can be two principal differences. First, the binding of ATP, ADP, or Pi and the dissociation of ATP, ADP, or Pi occur much more slowly. Second, the continuous decrease in the potential, which occurs as the ATP hydrolysis or synthesis proceeds and S1 moves along F-actin in Sect. 3.2 and case (1), is absent. Therefore, S1 feels the potential of red curve for a substantially long time, with the result that the movement of S1 is no more unidirectional (see Sect. 3.2.4).

As for AcrB, if the proton concentrations in the two sides are the same, the unidirectional, functional rotation does not occur and the efflux of drugs is no more successful. The discussions given in Sects. 4.4 and 4.5 are quite speculative but intriguing. They should be examined in further studies.

4.6 Changes in Thermodynamic Quantities upon Self-assembly Processes Measured in Experiments

Many of the existing experimental data show that the changes in enthalpy and entropy upon protein folding [5], amyloid-fibril formation [6], receptor-ligand binding [7], virus association [8], formation of F-actin by G-actin molecules [9], and binding of myosin to F-actin [10, 11] are both positive. This indicates that these processes are entropically driven. Even when the measured changes in enthalpy and entropy upon a self-assembly process are both negative, the process is not always enthalpically driven. Note that the experimental measurement is performed under isobaric condition. In cases where two hydrophobic solutes bind to each other, for example, part of the entropic gain, which would occur under isochoric condition, is converted to a corresponding decrease in enthalpy through the compression of bulk water [12–15]. Unfortunately, the effect of the compression of bulk water is not noticed in the biological research community.

4.7 Correct Interpretation of Hydrophobic Effect

According to the conventional view, the water near nonpolar groups is unstable in terms of entropy due to the water structuring (e.g., so-called iceberg structure near a nonpolar surface [16]). A self-assembly process is driven by the decrease in the amount of such unstable water (i.e., release of part of such unstable water to the bulk), which is referred to as "hydrophobic effect" [17]. On the other hand, we have been investigating the hydrophobic effect by decomposing the hydration entropy of a nonpolar solute into solute-water pair and many-body correlation components and further decomposing each component into two terms which are dependent on the excluded volume and on the area and curvatures of the water-accessible surface, respectively. The resultant four constituents are physically quite insightful. These decompositions, which are unique to our investigation, have provided a significant amount of new information [18, 19]. In our view, the reduction in water crowding in the entire system upon a self-assembly process is the dominant factor of the hydrophobic effect.

The structures formed by the self-assembly processes are collapsed by the application of high pressures. The power of forming the structures becomes considerably weaker at low temperatures. Typical examples in the former are denaturation of a protein, dissociation of filamentous actin (F-actin) into actin monomers [20, 21], destruction of amyloid fibril [22], and dissociation of virus assemblies [8] at high pressures. As those in the latter, a protein is unfolded, binding of myosin to F-actin is weakened [23], protein aggregation is dissociated [24], solubility of methane increases [25–27], and for nonionic amphiphilic molecules [28] the critical micelle concentration becomes higher and the average size of micelles becomes smaller at low temperatures. These phenomena suggest that there are common features of the self-assembly processes and a certain physical factor universally plays dominant roles as the driving force. We have shown that these pressure and temperature dependences of the hydrophobic effect can be elucidated only by our view [18, 19].

In the conventional view, a self-assembly process is largely driven by the hydrophobic effect. We agree with the dominance of the hydrophobic effect. However, it is implemented not through the contact of nonpolar groups but through the reduction of water crowding. In our view, in the protein-protein binding, for instance, the high shape complementarity on the atomic level (not necessarily for nonpolar residues) within the protein-protein interface is the most important [14, 15]. As long as the conventional view is replaced by our view, we can express that the hydrophobic effect is crucially important in the ordering processes as well as in the self-assembly processes.

4.8 Life and Translational, Configurational Entropy of Water

It is often emphasized that the formation of intramolecular hydrogen bonds, contact of unlike-charged atoms or groups, and packing of atoms providing van der Waals attractive interactions within a biomolecule play important roles in

biological self-assembly. However, it should be noted that these processes accompany the losses of water-biomolecule hydrogen bonds, electrostatic stabilization between positively charged atoms and water oxygens or negatively charged atoms and water hydrogens, and water-biomolecule van der Waals attractive interactions. This negative effect, which we refer to as the dehydration penalty, is significantly large. Even when the effect of the structure reorganization of water is taken into account, except for the van der Waals component, the net change in energy is positive in most cases [14, 15, 29]. As for the electrostatic interaction between solutes with like or unlike partial charges, which are exposed to aqueous solution, it becomes about two orders of magnitude weaker and much shorter ranged than in vacuum [30].

Here are the answers to the two questions raised in Chap. 1. The self-assembly and ordering processes in biological systems do not occur at the great expense of system entropy. They occur to increase the system entropy, which can be appreciated only by accounting for the water molecules which coexist with the biomolecules. Water is imperative in sustaining life in a variety of ways, but the most striking role of water is probably its entropic effect arising from the translational displacement of water molecules (i.e., effect of the translational, configurational entropy of water or the *true* hydrophobic effect driving a variety of self-assembly processes and the functional expression of molecular machines).

References

1. R. Ananthakrishnan, A. Ehrlichter, Int. J. Biol. Sci. **3**, 303 (2007)
2. H. Mishima, H. Oshima, S. Yasuda, M. Kinoshita, J. Phys. Chem. B **119**, 3423 (2015)
3. H. Noji, R. Yasuda, M. Yoshida, K. Kinosita Jr., Nature **386**, 299 (1997)
4. R. Yasuda, H. Noji, K. Kinosita Jr., M. Yoshida, Cell **93**, 1117 (1998)
5. N. Baden, S. Hirota, T. Takabe, N. Funasaki, M. Terazima, J. Chem. Phys. **127**, 175103 (2007)
6. J. Kardos, K. Yamamoto, K. Hasegawa, H. Naiki, Y. Goto, J. Biol. Chem. **279**, 55308 (2004)
7. H. Ohtaka, A. Schon, E. Freire, Biochemistry **42**, 13659 (2003)
8. C.F.S. Bonafe, C.M.R. Vital, R.C.B. Telles, M.C. Goncalves, M.S.A. Matsuura, F.B.T. Pessine, D.R.C. Freitas, J. Vega, Biochemistry **37**, 11097 (1998)
9. F. Oosawa, S. Asakura, *Thermodynamics of the Polymerization of Protein* (Academic, New York, 1975)
10. T. Kodama, Physiol. Rev. **65**, 467 (1985)
11. T. Katoh, F. Morita, J. Biochem. **120**, 189 (1996)
12. N.M. Cann, G.N. Patey, J. Chem. Phys. **106**, 8165 (1997)
13. M. Kinoshita, Y. Harano, R. Akiyama, J. Chem. Phys. **125**, 244504 (2006)
14. T. Hayashi, H. Oshima, T. Mashima, T. Nagata, M. Katahira, M. Kinoshita, Nucleic Acids Res. **42**, 6861 (2014)
15. T. Hayashi, H. Oshima, S. Yasuda, M. Kinoshita, J. Phys. Chem. B **119**, 14120 (2015)
16. W. Kauzmann, Adv. Protein Chem. **14**, 1 (1959)
17. K.A. Dill, Biochemistry **29**, 7133 (1990)
18. M. Kinoshita, Biophys. Rev. **5**, 283 (2013)
19. H. Oshima, M. Kinoshita, J. Chem. Phys. **142**, 145103 (2015)
20. T. Ikkai, T. Ooi, Biochemistry **5**, 1551 (1966)

21. P.S. Niranjan, P.B. Yim, J.G. Forbes, S.C. Greer, J. Dudowicz, K.F. Freed, J.F. Douglas, J. Chem. Phys. **119**, 4070 (2003)
22. D. Foguel, M.C. Suarez, A.D. Ferrao-Gonzales, T.C.R. Porto, L. Palmieri, C.M. Einsiedler, L.R. Andrade, H.A. Lashuel, P.T. Lansbury, J.W. Kelly, J.L. Silva, Proc. Natl. Acad. Sci. U.S.A. **100**, 9831 (2003)
23. S. Highsmith, Arch. Biochem. Biophys. **180**, 404 (1977)
24. R. Mishra, R. Winter, Angew. Chem. Int. Ed. **47**, 6518 (2008)
25. M. Kinoshita, J. Chem. Phys. **128**, 024507 (2008)
26. B. Widom, P. Bhimalapuram, K. Koga, Phys. Chem. Chem. Phys. **5**, 3085 (2003)
27. H.S. Ashbaugh, L.R. Pratt, Rev. Mod. Phys. **78**, 159 (2006)
28. D. Myres, *Surfaces, Interfaces, and Colloids: Principles and Applications* (Wiley-VCH, Berlin, 1999)
29. T. Yoshidome, M. Kinoshita, S. Hirota, N. Baden, M. Terazima, J. Chem. Phys. **128**, 225104 (2008)
30. M. Kinoshita, Y. Harano, Bull. Chem. Soc. Jpn **78**, 1431 (2005)